U.S. DEPARTMENT OF COMMERCE
NATIONAL OCEANIC AND ATMOSPHERIC
ADMINISTRATION
NATIONAL WEATHER SERVICE

Environmental Modeling Center
Ocean Modeling Branch

TECHNICAL NOTE [1]

NUMERICAL MODELING OF SURFACE WAVES BASED ON PRINCIPAL EQUATIONS OF POTENTIAL WAVE DYNAMICS

D. Chalikov, D. Sheinin

December 4, 1996

This is an unreviewed manuscript, intended for informal exchange of information

[1]OMB contribution number No. 139

OPC CONTRIBUTIONS

No. 1. Burroughs, L. D., 1987: Development of Forecast Guidance for Santa Ana Conditions. National Weather Digest, Vol. 12 No. 1, 7pp.

No. 2. Richardson, W. S., D. J. Schwab, Y. Y. Chao, and D. M. Wright, 1986: Lake Erie Wave Height Forecasts Generated by Empirical and Dynamical Methods -- Comparison and Verification. Technical Note, 23pp.

No. 3. Auer, S. J., 1986: Determination of Errors in LFM Forecasts Surface Lows Over the Northwest Atlantic Ocean. Technical Note/NMC Office Note No. 313, 17pp.

No. 4. Rao, D. B., S. D. Steenrod, and B. V. Sanchez, 1987: A Method of Calculating the Total Flow from A Given Sea Surface Topography. NASA Technical Memorandum 87799., 19pp.

No. 5. Feit, D. M., 1986: Compendium of Marine Meteorological and Oceanographic Products of the Ocean Products Center. NOAA Technical Memorandum NWS NMC 68, 93pp.

No. 6. Auer, S. J., 1986: A Comparison of the LFM, Spectral, and ECMWF Numerical Model Forecasts of Deepening Oceanic Cyclones During One Cool Season. Technical Note/NMC Office Note No. 312, 20pp.

No. 7. Burroughs, L. D., 1987: Development of Open Fog Forecasting Regions. Technical Note/NMC Office Note. No. 323., 36pp.

No. 8. Yu, T. W., 1987: A Technique of Deducing Wind Direction from Satellite Measurements of Wind Speed. Monthly Weather Review, 115, 1929-1939.

No. 9. Auer, S. J., 1987: Five-Year Climatological Survey of the Gulf Stream System and Its Associated Rings. Journal of Geophysical Research, 92, 11,709-11,726.

No. 10. Chao, Y. Y., 1987: Forecasting Wave Conditions Affected by Currents and Bottom Topography. Technical Note, 11pp.

No. 11. Esteva, D. C., 1987: The Editing and Averaging of Altimeter Wave and Wind Data. Technical Note, 4pp.

No. 12. Feit, D. M., 1987: Forecasting Superstructure Icing for Alaskan Waters. National Weather Digest, 12, 5-10.

No. 13. Sanchez, B. V., D. B. Rao, and S. D. Steenrod, 1987: Tidal Estimation in the Atlantic and Indian Oceans. Marine Geodesy, 10, 309-350.

No. 14. Gemmill, W. H., T. W. Yu, and D. M. Feit 1988: Performance of Techniques Used to Derive Ocean Surface Winds. Technical Note/NMC Office Note No. 330, 34pp.

No. 15. Gemmill, W. H., T. W. Yu, and D. M. Feit 1987: Performance Statistics of Techniques Used to Determine Ocean Surface Winds. Conference Preprint, Workshop Proceedings AES/CMOS 2nd Workshop of Operational Meteorology. Halifax, Nova Scotia., 234-243.

No. 16. Yu, T. W., 1988: A Method for Determining Equivalent Depths of the Atmospheric Boundary Layer Over the Oceans. Journal of Geophysical Research. 93, 3655-3661.

No. 17. Yu, T. W., 1987: Analysis of the Atmospheric Mixed Layer Heights Over the Oceans. Conference Preprint, Workshop Proceedings AES/CMOS 2nd Workshop of Operational Meteorology, Halifax, Nova Scotia, 2, 425-432.

No. 18. Feit, D. M., 1987: An Operational Forecast System for Superstructure Icing. Proceedings Fourth Conference Meteorology and Oceanography of the Coastal Zone. 4pp.

No. 19. Esteva, D. C., 1988: Evaluation of Priliminary Experiments Assimilating Seasat Significant Wave Height into a Spectral Wave Model. Journal of Geophysical Research. 93, 14,099-14,105.

No. 20. Chao, Y. Y., 1988: Evaluation of Wave Forecast for the Gulf of Mexico. Proceedings Fourth Conference Meteorology and Oceanography of the Coastal Zone, 42-49.

Numerical modeling of surface waves based on principal equations of potential wave dynamics[2]

D. Chalikov[a] & D. Sheinin[b]

[a] UCAR Visiting Scientist, Ocean Modeling Branch/NCEP, 5200 Auth Road, Camp Spring, MD 20746, USA
[b] Massachussets Institute of Technology, Bldg E40-259, 1 Amherst st., Cambridge, MA 02139, USA

Abstract

A method for numerical investigation of nonlinear wave dynamics based on direct hydrodynamical modeling of 1-D potential periodic surface waves is presented. By a nonstationary conformal mapping, the principal equations are rewritten in a surface-following coordinate system and reduced to two simple evolutionary equations for the elevation and the velocity potential of the surface. For stationary equations, the proposed approach coincides with the conventional complex variable method. For this case, numerical algorithms for solution of gravity (Stokes) and gravity-capillary wave equations are proposed, and examples of numerical solutions are given. The results imply that gravity-capillary waves do not approach Stokes waves as the capillarity coefficient decreases. Both stationary and nonstationary schemes use Fourier series representation for spatial approximation and the Fourier transform method to calculate nonlinearities. The nonstationary model was validated by simulation of propagating waves with initial conditions obtained as numerical (for gravity and gravity-capillary waves) or analytical (for pure capillary, or Crapper's waves) solutions of the stationary problem. The simulated progressive waves did not change their shape during long-term time integration, which indicates high accuracy of the scheme. Another criterion used for model validation was conservation of integral invariants of simulated multi-mode wave fields. A number of long-term model simulations of gravity, gravity-capillary, and pure capillary waves, with various initial conditions, were performed; for the simulated wave fields, distributions of energy and phase speed over spectra were analyzed. It was found that the wavenumber-frequency spectra are well separated into patterns lying along regularly located curves, with most of the energy concentrated along the curves corresponding to free and bound waves. This set of curves can be described by the equation $D(\omega/n, k/n) = 0$ $(n = 1, 2, 3, ...)$, where

[2]OMB contibution no. 131

$D(\omega, k) = 0$ is approximated by the linear dispersion relation but does not coincide with it, especially for large k where there is a tendency for the indicated equation to approximate a straight line. Some other properties of simulated wave fields were also analyzed; these included temporal evolution of the spectra and spatial distribution of the energy of perturbations. The method developed may be applied to a broad range of problems where the assumption of one-dimensionality is acceptable.

1. Introduction

Computational techniques for numerical solution of the Navier-Stokes equations have brought new developments to geophysical fluid dynamics. Using modern numerical models, the long-term evolution of several complicated dynamical phenomena in different fluids, including the atmosphere, can be successfully simulated. However, the long-term simulation of a nonlinear multi-mode wave field is difficult to perform, since most numerical schemes for the Euler equations fail to provide sufficient accuracy for treating nonlinearities in wave motion. The main source of error is primarily due to the finite difference representation of the vertical structure of the flow when waves with different wave numbers are present. Thus, theoretical and numerical investigations of surface gravity waves are usually based on the equations for potential flow with a free surface. In this case the flow is fully determined by the form of the surface and the velocity potential on the surface and in its vicinity. The potential motion assumption, of course, idealizes the phenomenon, since actual wave motion is both rotational and turbulent. Fortunately, potential theory gives many results which agree well with observations. For example, it is well-known that even linear theory yields phase velocity estimates with an accuracy of the order of 1% . A much more sophisticated theory, dealing with nonlinear wave-wave interactions (Hasselman,1962) which is also based on the potential motion assumption, gives results which are confirmed by experimental data.

The main advantage of the potential motion approximation is that the system of Euler dynamical equations is reduced to Laplace equation. However, the solution to the problem of surface wave motion is complicated by the requirement of having to apply the kinematic and dynamic boundary conditions (both nonlinear) on the free surface, the location of which is unknown at any given moment. Some attempts have been made

previously to reproduce the evolution of waves in a Cartesian coordinate system (e.g. Prosperetti and Jacobs, 1983), but such techniques are not applicable to long-term integrations. A more feasible approach is based on a formulation of the governing equations in a surface-following coordinate system; the simplest technique uses the difference between the Cartesian vertical coordinate and the surface height as the new vertical coordinate, along with Cartesian coordinates in the horizontal. However, this does not eliminate all of the problems, since the Laplace equation is transformed into a general elliptic equation, and an integral equation must be solved at each time step (Chalikov and Liberman, 1991) to calculate the vertical derivative of the velocity potential. Another approach is based on expanding the velocity potential in power series in the vicinity of the surface. Such a method, developed by Watson and West (1975), was applied to the solution of the two-dimensional potential wave equations (West et al., 1987). Even though this model gave excellent results for a relatively small number of modes, the method is not universal since the convergence of the power series is slow for the case of multi-mode wave field with typical spectral energy distribution.

In this study we consider only 1-D nonlinear waves. Such waves were simulated numerically with a quasi-Lagrangian technique (Longuet-Higgins and Cokelet, 1976), and with a Cauchy-type integral algorithm (Dold, 1991). The performance of neither scheme was limited by wave steepness, and both were capable of simulating the initial phase of wave breaking (a phenomenon whose later stages are rotational and remain extremely difficult to simulate directly). A method based on a Taylor expansion of the Dirichlet-Neumann operator was developed by Craig and Sulem (1993). The method was illustrated by computing evolution of modulated wave packets and a low order approximation of the Stokes wave for relatively short periods. However, the applicability of these methods to simulating longer time scales is uncertain.

Our goal is to construct a numerical scheme for direct modeling of 1-D potential waves so that the effects of nonlinear interactions on time scales much longer than the wave period may be analyzed. The approach is based on a nonstationary conformal mapping which allows us to rewrite the equations of potential waves (which take into account the effect of capillarity and finite depth) in a surface-following coordinate system, where the Laplace equation retains its form, so that the original sys-

tem can be represented by two relatively simple evolutionary equations (section 2). These equations may be solved by using Fourier transform method with high accuracy and computational efficiency. Section 3 deals with stationary solutions of the system; a numerical method to obtain stationary gravity (Stokes) and gravity-capillary waves is presented and results of the computations are discussed. The numerical scheme for the nonstationary equations is described in section 4. The results of section 3, as well as mass, momentum and energy conservation criteria, are used for validation of the nonstationary model (section 5). In section 6, results of long-term model simulations are discussed, and spectral properties of the obtained wave fields are analyzed.

2. Equations

Consider the principal 2-D equations for potential waves written in Cartesian coordinates, i.e. the Laplace equation for the velocity potential Φ

$$\Phi_{xx} + \Phi_{zz} = 0 \ , \tag{1}$$

and the two boundary conditions at the free surface $z = h(x,t)$: the kinematic condition

$$h_t + h_x \Phi_x - \Phi_z = 0 \ , \tag{2}$$

and the Lagrange integral

$$\Phi_t + \frac{1}{2}\left(\Phi_x^2 + \Phi_z^2\right) + h + p - \sigma h_{xx}(1 + h_x^2)^{-3/2} = 0 \ , \tag{3}$$

where p is the external surface pressure. [2]

The equations are to be solved in the domain

$$-\infty < x < \infty, \ \ -H \le z \le h(x,t) \ . \tag{4}$$

The variables Φ and h are considered to be periodic with respect to x , the period being 2π, and a zero normal velocity condition at the bottom is assumed:

[2]Subscripts of independent variables denote partial differentiation with respect to this variable.

$$\Phi_z(x, z = -H, t) = 0 \tag{5}$$

Equations (1)-(3) are written in non-dimensional form, with the following scales: length L, where $2\pi L$ is the (dimensional) period in the horizontal, time $\mathcal{T} = L^{1/2} g^{-1/2}$, and the velocity potential $L^{3/2}\mathrm{g}^{1/2}$ (g - acceleration of gravity). The last term in (3) describes the effect of surface tension, and

$$\sigma = \frac{\Gamma}{g\, L^2} \ , \tag{6}$$

is a nondimensional parameter. ($\Gamma \simeq 8 \cdot 10^{-5} m^3 s^{-2}$ is the kinematic coefficient of surface tension for water).

System (1)-(3) is solved as an initial value problem for the unknown functions Φ and h with given initial conditions $\Phi(x, z = h(x, t = 0), t = 0)$ and $h(x, t = 0)$. However, straightforward numerical integration of this system is known to be computationally inefficient and, for time periods much greater than the time scale $\mathcal{T}$, virtually impracticable. To make a numerical solution feasible, we introduce a surface-following coordinate system which conformally maps the original domain (4) onto the strip

$$-\infty < \xi < \infty, \ \ -\tilde{H} \le \zeta \le 0 \ , \tag{7}$$

with a periodicity condition given as

$$\begin{array}{rcl} x(\xi, \zeta, \tau) & = & x(\xi + 2\pi, \zeta, \tau) + 2\pi \\ z(\xi, \zeta, \tau) & = & z(\xi + 2\pi, \zeta, \tau) \ , \end{array} \tag{8}$$

where τ is the new time coordinate, $\tau = t$. (Note that the mapping is time-dependent, since it involves the surface height h).

It can readily be shown that a required conformal mapping exists and, due to periodicity condition (8), can be represented through Fourier series:

$$x = \xi + x_0(\tau) + \sum_{-M \le k \le M, k \ne 0} \eta_{-k}(\tau) \frac{\cosh k(\zeta + \tilde{H})}{\sinh k\tilde{H}} \vartheta_k(\xi) \ , \tag{9}$$

$$z = \zeta + \eta_0(\tau) + \sum_{-M \le k \le M, k \ne 0} \eta_k(\tau) \frac{\sinh k(\zeta + \tilde{H})}{\sinh k\tilde{H}} \vartheta_k(\xi) \ , \tag{10}$$

where η_k are the coefficients of Fourier expansion of the free surface $\eta(\xi,\tau)$ with respect to the new horizontal coordinate ξ:

$$\eta(\xi,\tau) = h(x(\xi,\zeta=0,\tau),t=\tau) = \sum_{-M\le k\le M} \eta_k(\tau)\vartheta_k(\xi) \ ; \tag{11}$$

ϑ_k denotes the function

$$\vartheta_k(\xi) = \begin{cases} \cos k\xi & k \ge 0 \\ \sin k\xi & k < 0 \end{cases} \tag{12}$$

(note that $(\vartheta_k)_\xi = k\vartheta_{-k}$, and $\sum(A_k\vartheta_k)_\xi = -\sum kA_{-k}\vartheta_{k\cdot}$); M is the truncation number to be used in numerical integration (so far $M=\infty$ is assumed); $x_0(\tau)$ can be chosen arbitrarily, though it is convenient to assume

$$x_0(\tau) = 0 \ . \tag{13}$$

The lower boundary $\zeta = -\tilde{H}$ cannot be chosen arbitrarily, since the relation

$$z(\xi,\zeta=-\tilde{H},\tau) = -H \tag{14}$$

must hold, which, after substituting (10), yields:

$$\tilde{H} = H + \eta_0(\tau) \ . \tag{15}$$

Since η_0 is determined by the Fourier expansion given by (11), and, generally, is an unknown function of time, $\tilde{H}$ also depends on time.

Due to the conformity of the mapping, Laplace equation (1) retains its form in (ξ,ζ) coordinates. Standard derivations show that system (1)-(3) can be written in the new coordinates as follows:

$$\Phi_{\xi\xi} + \Phi_{\zeta\zeta} = 0 \tag{16}$$

$$-z_\xi x_\tau + x_\xi z_\tau = \Phi_\zeta \tag{17}$$

$$\begin{aligned} \Phi_\tau - J^{-1}(x_\xi x_\tau + z_\xi z_\tau)\Phi_\xi + \frac{1}{2}J^{-1}(\Phi_\xi^2 - \Phi_\zeta^2) \\ +z + p - \sigma J^{-3/2}(-x_{\xi\xi}z_\xi + z_{\xi\xi}x_\xi) = 0 \end{aligned} \tag{18}$$

where (17) and (18) are written for the surface $\zeta = 0$ (so that $z = \eta$ as represented by (11)), and

$$J = x_\xi^2 + z_\xi^2 = x_\zeta^2 + z_\zeta^2 \tag{19}$$

is the Jacobian of the transformation.

Boundary condition (5) readily yields:

$$\Phi_\zeta(\xi, \zeta = -\tilde{H}, \tau) = 0 \ . \tag{20}$$

The Laplace equation (16) with boundary condition (20) is solved via Fourier expansion (which reduces system (16)-(18) to a 1-D problem):

$$\Phi = \sum_{-M \le k \le M} \phi_k(\tau) \frac{\cosh k(\zeta + \tilde{H})}{\cosh k\tilde{H}} \vartheta_k(\xi) \ , \tag{21}$$

where ϕ_k are Fourier coefficients of the surface potential $\Phi(\xi, \zeta = 0, \tau)$. Thus, (17) and (18) constitute a closed system of prognostic equations for the surface functions $z(\xi, \zeta = 0, \tau) = \eta(\xi, \tau)$ and $\Phi(\xi, \zeta = 0, \tau)$. In principle, it can be written as a system of ordinary differential equations for the Fourier coefficients η_k, ϕ_k using (11) and the following formulae which are easily obtained from (9), (10), (12), (13), (15), (21):

$$\Phi(\xi, \zeta = 0, \tau) = \sum_{-M \le k \le M} \phi_k(\tau) \vartheta_k(\xi) \tag{22}$$

$$\Phi_\xi(\xi, \zeta = 0, \tau) = - \sum_{-M \le k \le M} k\phi_{-k}(\tau) \vartheta_k(\xi) \tag{23}$$

$$\Phi_\zeta(\xi, \zeta = 0, \tau) = \sum_{-M \le k \le M} k\phi_k(\tau) \tanh\left(k\tilde{H}\right) \vartheta_k(\xi) \tag{24}$$

$$x_\xi(\xi, \zeta = 0, \tau) = 1 + \sum_{-M \le k \le M, k \ne 0} k\eta_k(\tau) \coth\left(k\tilde{H}\right) \vartheta_k(\xi) \tag{25}$$

$$z_\xi(\xi, \zeta = 0, \tau) = - \sum_{-M \le k \le M} k\eta_{-k}(\tau) \vartheta_k(\xi) \tag{26}$$

$$x_{\xi\xi}(\xi, \zeta = 0, \tau) = - \sum_{-M \le k \le M, k \ne 0} k^2\eta_{-k}(\tau) \coth\left(k\tilde{H}\right) \vartheta_k(\xi) \tag{27}$$

$$z_{\xi\xi}(\xi, \zeta = 0, \tau) = - \sum_{-M \le k \le M} k^2\eta_k(\tau) \vartheta_k(\xi) \tag{28}$$

$$\Phi_\tau(\xi,\zeta=0,\tau)=\sum_{-M\le k\le M}\dot{\phi}_k(\tau)\vartheta_k(\xi) \tag{29}$$

$$x_\tau(\xi,\zeta=0,\tau)=\sum_{-M\le k\le M,k\neq 0}\left(\dot{\eta}_{-k}(\tau)\coth\left(k\tilde{H}\right)-\frac{k\eta_{-k}(\tau)\dot{\eta}_0(\tau)}{\sinh^2(k\tilde{H})}\right)\vartheta_k(\xi) \tag{30}$$

$$z_\tau(\xi,\zeta=0,\tau)=\sum_{-M\le k\le M}\dot{\eta}_k(\tau)\vartheta_k(\xi) \tag{31}$$

System (17), (18) is not resolved with respect to the time derivative of the surface elevation $\eta(\xi,\tau)$. During numerical integration of the initial value problem, the values of the time derivative can be obtained with a simple iterative algoritm making use of (17) and Cauchy-Riemann relations $x_{\tau\xi}=z_{\tau\zeta}$, $x_{\tau\zeta}=-z_{\tau\xi}$. However, a more efficient approach may be applied (V. Zakharov, private communication; see also Kuznetsov et al., 1994). Introducing complex variables $\rho=\xi+\mathrm{i}\zeta$ and denoting $r(\rho,\tau)=x(\xi,\zeta,\tau)+\mathrm{i}z(\xi,\zeta,\tau)$, we can rewrite the left-hand side of equation (17) as follows

$$Im\left(\frac{r_\tau}{r_\rho}\right)_{\zeta=0}=\left(J^{-1}\Phi_\zeta\right)_{\zeta=0} \tag{32}$$

Note that due to conformity of the transformation, $r(\rho,\tau)$ is an analytic function of ρ, and so are $r_\tau=x_\tau+\mathrm{i}z_\tau$, $r_\rho=x_\xi+\mathrm{i}z_\xi$, and their ratio in the left-hand side of (32). Therefore, if we denote

$$\frac{r_\tau}{r_\rho}=F(\xi,\zeta,\tau)+\mathrm{i}G(\xi,\zeta,\tau)\ , \tag{33}$$

functions F and G are bound by the Cauchy-Riemann relations:

$$F_\xi=G_\zeta\ ,\quad F_\zeta=-G_\xi\ . \tag{34}$$

Considering that G is a harmonic function of ξ and ζ, and that it becomes zero at the lower boundary $\zeta=-\tilde{H}$ (because at that boundary $z=-H$, $z_\tau=z_\xi=0$), so that

$$(F+\mathrm{i}G)_{\zeta=-\tilde{H}}=\left(\frac{x_\tau}{x_\xi}\right)_{\zeta=-\tilde{H}}=(F)_{\zeta=-\tilde{H}}\ , \tag{35}$$

we can write the following expansion:

$$G(\xi,\zeta,\tau) = \sum_{-M\le k\le M, k\neq 0} g_k(\tau)\frac{\sinh k(\zeta+\tilde{H})}{\sinh k\tilde{H}}\vartheta_k(\xi) \ , \qquad (36)$$

and (34) yield:

$$F(\xi,\zeta,\tau) = f_0(\tau) + \sum_{-M\le k\le M, k\neq 0} g_{-k}(\tau)\frac{\cosh k(\zeta+\tilde{H})}{\sinh k\tilde{H}}\vartheta_k(\xi) \ . \qquad (37)$$

Function $f_0(\tau)$ can be found using assumption (13), which together with (33) yields (for any ζ and τ):

$$0 = \int_0^{2\pi} x_\tau d\xi = \int_0^{2\pi} (Fx_\xi - Gz_\xi)d\xi \ ;$$

substituting (36), (37), (9), (10), and integrating the products of the Fourier series, we obtain:

$$f_0 = \frac{1}{2}\sum_{-M\le k\le M, k\neq 0} k\eta_{-k}g_k \sinh^{-2}(k\tilde{H}) \ . \qquad (38)$$

Then if

$$g(\xi,\tau) = G(\xi,\zeta=0,\tau) = \sum_{-M\le k\le M, k\neq 0} g_k(\tau)\vartheta_k(\xi) \qquad (39)$$

is known,

$$f(\xi,\tau) = F(\xi,\zeta=0,\tau) = f_0(\tau) + \sum_{-M\le k\le M, k\neq 0} g_{-k}(\tau)\coth(k\tilde{H})\vartheta_k(\xi) \qquad (40)$$

is also known: f is a generalization of the Hilbert transform of g, which, for $k \neq 0$, may be defined in Fourier space as

$$f_k = g_{-k}\coth(k\tilde{H}) \ , \quad g_k = -f_{-k}\tanh(k\tilde{H}) \ , \qquad (41)$$

whereas $g_0 = 0$ and f_0 is defined by (38). Thus, we can replace equation (17) by explicit expressions for the time derivatives x_τ and z_τ which follow from (33). Finally, (17) and (18) can be rewritten as a system which is resolved with respect to the time derivatives (here $\zeta = 0$):

$$z_\tau = x_\xi g + z_\xi f \qquad (42)$$

$$\Phi_\tau = f\Phi_\xi - \frac{1}{2}J^{-1}(\Phi_\xi^2 - \Phi_\zeta^2) - z - p + \sigma J^{-3/2}(-x_{\xi\xi}z_\xi + z_{\xi\xi}x_\xi) \ , \quad (43)$$

where according to (32),

$$g = \left(J^{-1}\Phi_\zeta\right)_{\zeta=0} \ , \quad (44)$$

f is obtained from g according to (38) - (40), and the derivatives can be expressed through Fourier series (22)-(29), (31) (eq. (30) is no longer needed, since x_τ has been eliminated from the system).

Thus, the original system of equations is transformed into two evolutionary equations (42), (43) which can be effectively solved using the Fourier transform method (see section 4).

For deep water ($H = \infty$), the expressions in (24), (25), (27), (30), (38), (40), (41) become simpler, since $\tanh(k\tilde{H})$ and $\coth(k\tilde{H})$ are replaced by $\mathrm{sign}(k)$, and the terms with $\sinh^{-2}(k\tilde{H})$ vanish. In particular, operator (41) becomes a conventional Hilbert transform, and (38) is reduced to $f_0 = 0$.

To include the case of pure capillary waves, it is convenient to use a different scaling: $L^{3/2}\Gamma^{-1/2}$ for time and $L^{1/2}\Gamma^{1/2}$ for velocity potential. With the new nondimensional variables, equations (43), (42) acquire the following form

$$z_\tau = x_\xi g + z_\xi f \quad (45)$$

$$\Phi_\tau = f\Phi_\xi - \frac{1}{2}J^{-1}(\Phi_\xi^2 - \Phi_\zeta^2) - \alpha z - p + J^{-3/2}(-x_{\xi\xi}z_\xi + z_{\xi\xi}x_\xi) \ , \quad (46)$$

where $\alpha = \sigma^{-1}$.

3. Stationary solutions

For the stationary problem, the method of conformal mapping is a well-known approach based on using the velocity potential Φ and the stream function Ψ as the independent variables (e.g. Crapper, 1984). It is easy to show that in this case

$$\Phi = -c\xi + \Phi_0, \quad \Psi = c\zeta + \Psi_0 \ , \tag{47}$$

where $-c$ is the velocity of the mean flow, $\Phi_x = -\Psi_z$ and $\Phi_z = \Psi_x$ are the horizontal and the vertical Cartesian velocity components respectively, and Φ_0 and Ψ_0 are constants.

For the stationary version of system (1) - (3) (or (16) - (18)) to describe progressive waves, the periodicity condition on Φ, which implies a zero mean flow velocity, must be replaced by the weaker condition of periodicity of the velocity components, i.e. of the spatial derivatives of Φ. In a coordinate system moving with the wave's phase velocity c, the mean flow velocity is equal to $-c$, and the velocity potential Φ is given by (47) where Φ_0 must be allowed to depend on time (since stationarity is assumed for the velocity field rather than the velocity potential). Consequently, with the external pressure $p = 0$, system (16) - (18) is reduced to one equation written for the surface $\zeta = 0$:

$$\frac{1}{2}c^2 J^{-1} + z - \sigma J^{-3/2}(-x_{\xi\xi}z_\xi + z_{\xi\xi}x_\xi) = a \tag{48}$$

where $a = -\frac{d\Phi_0}{d\tau}$, and since the left-hand side of (48) does not depend on time, a is a constant (so that the dependence of Φ_0 on τ may only be linear).

In this work, eq. (48) is solved numerically using Fourier expansions (9), (10) for x and z, and (25)-(28) for the derivatives in (48), (19). The nonlinearities are evaluated at gridpoints $\xi^{(j)} = 2\pi(j-1)/N$, N being the total number of gridpoints. This approach, developed by Orszag (1970) and Elliassen (1970) is known as transform method and is discussed in more detail in section 4.

Note that because σ is a factor in a term having the highest differential order, we may face effects of singularity for small σ. Indeed, we had to develop two different schemes for the cases of pure gravity and gravity-capillary waves, and it will be seen that in the latter case the numerical solution does not approach a Stokes wave as σ decreases.

Below we consider only the case of deep water ($H = \infty$); however, generalization of the algorithms described in the following subsections is

straightforward for the case of a finite depth.

3.1 Pure gravity waves.

With $\sigma = 0$, the solutions of equation (48) are Stokes waves. A method based on expansion of the Fourier coefficients of the surface height in power series of the wave amplitude was initially proposed by Stokes (1847, 1880) who in his latter work obtained a fifth-order approximation. In recent studies, the method has been further developed into a computer-oriented recursive scheme which produces consecutive power expansion coefficients; Drennan et al. (1992) carried out the power series calculations up to 170 terms.

Here, the solutions in the form of Fourier expansion coefficients for the surface height were sought numerically with an iterative algorithm. The conformal mapping with surface boundary condition (48) is determined by the coefficients η_k through the relationships

$$x(\xi,\zeta) = \xi + \sum_{-M\le k\le M, k\neq 0} \eta_{-k} \exp(k\zeta)\vartheta_k(\xi) \tag{49}$$

$$z(\xi,\zeta) = \zeta + \sum_{-M\le k\le M} \eta_k \exp(k\zeta)\vartheta_k(\xi) \tag{50}$$

which are the stationary deep-water versions of (9), (10). With $\zeta = 0$, (49) and (50) may serve as a parametric representation of the surface.

For pure gravity waves, equation (48) can be rewritten in the form

$$\log(\frac{1}{2}c^2) - \log J = \log(a - z) \ . \tag{51}$$

Denoting $w = \frac{d\log r}{d\rho}$ with r , ρ defined as in (32), it is can be seen that

$$\log J = 2Re(w), \quad z_\xi = Im(\exp w) \ . \tag{52}$$

Thus, if the Fourier expansion for $\log J$ is known, $Im(w)$ (also in the Fourier space) can be found via the Hilbert transform as in the second of the equalities (41), after which w and then $\exp w$ can be calculated at the gridpoints. This yields z_ξ, and after finding the corresponding Fourier coefficients by direct Fourier transform, z can be obtained by integration in Fourier space. Thus, z can be easily found if $\log J$ is known. This allows us to reduce the differential relationship (51) to an equation with

an integral operator, which may be solved by a simple iterative procedure.

Assuming that z is an even function of ξ , it is convenient to choose

$$s = \frac{1}{4}(\log J(\xi = 0, \zeta = 0) - \log J(\xi = \pi, \zeta = 0)) \qquad (53)$$

as the parameter determining the amplitude of the wave (in linear approximation, s is equal to the amplitude). With $\chi^{[n]}$ denoting the value of any variable χ on n-th iteration, the scheme can be written as follows:

G1. Assume $n = 0$, $\log J^{[0]} = 2s\ e^{\zeta} \cos\xi$ (this is the solution of the linearized problem).

G2. For given $\log J^{[n]}$, use Hilbert transform (41), complex exponent calculation, and integration in Fourier space to find $z^{[n]}$ as described above. If the maximum surface gridpoint value of $\mid z^{[n]} - z^{[n-1]} \mid$ is less than the prescribed accuracy ϵ, the iterations are completed, and $z^{[n]}$ is an approximate solution within the accuracy given.

G3. Let

$$a = a^{[n+1]} = \frac{e^{4s} z^{[n]}(\xi = 0) - z^{[n]}(\xi = \pi)}{e^{4s} - 1} \ .$$

This will ensure relation (53) for the next iteration. Calculate sufrace gridpoint values of

$$\log J^{[n+1]} = -\log(a^{[n+1]} - z^{[n]}) + (\log(a^{[n+1]} - z^{[n]}))_0 \qquad (54)$$

where $()_0$ denotes mean over ξ , i.e. 0-th Fourier coefficient.

G4. Find the Fourier expansion of $\log J^{[n+1]}$ by a Fourier transform; let $n = n + 1$ and return to step G2.

The last term in (54) allows us to find the phase velocity on $(n+1)$-st iteration: in accordance with (51), this term is equal to $\log\left(\frac{1}{2}(c^{[n+1]})^2\right)$. Equality (54) is based on the fact that the mean value of $\log J$ over ξ is zero, which follows from the first of relations (52), as $w \to 0$ when $\zeta \to -\infty$.

Fig. 1 illustrates some results of the described procedure for $M = 384$, $N = 1728$, $\epsilon = 10^{-11}$. The values of the parameter s for the given profiles

are 0.04, 0.08, 0.16, 0.32, 1.06. The number of iterations varied from 28 for $s = 0.04$ to 44 for $s = 1.06$. For $s = 1.06$, the amplitude

$$A = \frac{1}{2}(\eta(\xi = 0) - \eta(\xi = \pi)) = \frac{1}{2}(h(x = 0) - h(x = \pi)) \qquad (55)$$

is approximately 0.4374 which is close to that of Stokes wave with maximum steepness (about 0.443 according to Longuet-Higgins, 1975).

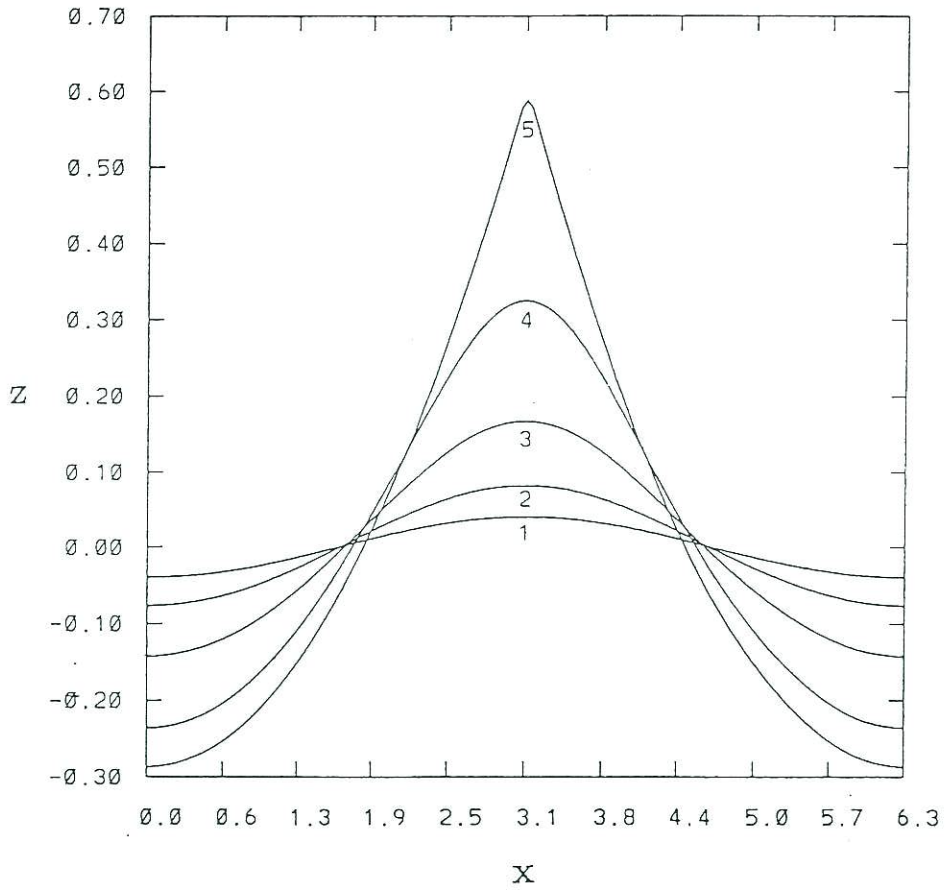

Figure 1: Profiles of Stokes waves: Curve 1 - $A = 0.0399$, 2 - $A = 0.0793$, 3 - $A = 0.1547$, 4 - $A = 0.2806$, 5 - $A = 0.4374$.

Theoretically, s can be arbitrarily large; $s = \infty$ for the steepest Stokes wave whose crest constitutes an angle of 120° and thus is a singularity with $J(\xi = 0, \zeta = 0) = \infty$. The algorithm does converge for values of s much larger than those used in Fig. 1; however, when the profile becomes close to that of the steepest wave, convergence of the Fourier

series slows down dramatically, and at the same time, due to strong nonlinearities, the accuracy of the transform method decreases sharply. As a result, for large s the numerical solution contains spurious oscillations; with the values of M, N indicated above, for $s > 1.06$ the maximum slope of the numerically obtained profile exceeds $30°$ for $s > 1.06$, which is a theoretical maximum.

When the iteration convergence criterium ϵ is small enough, the error of the method is the truncation error, which can be evaluated by comparison of results obtained with different resolutions. Such a comparison was carried out for three resolutions: $M = 384$, $N = 1728$; $M = 192$, $N = 864$; $M = 96$, $N = 432$. The results are illustrated in Table 1, where A_M is the value of the amplitude A (as defined in (55)) obtained with the truncation number M; $MAXD_{M_1,M_2}$ is the maximum gridpoint value for the distance

$$R = \left((x_{M_1} - x_{M_2})^2 + (z_{M_1} - z_{M_2})^2\right)^{1/2} \quad , \tag{56}$$

where $x_M = x_M(\xi)$, $z_M = z_M(\xi)$ is the numerical solution for x, z at $\zeta = 0$ obtained with the truncation number M;

$$RMSD_{M_1,M_2} = \left(\frac{1}{2\pi}\int_0^{2\pi} (R(\xi))^2 d(x(\xi))\right)^{1/2} \tag{57}$$

is the root mean square difference over x coordinate.

Table 1 shows that for amplitudes $A < 0.4$ the truncation errors are very small for all tested resolutions and decrease rapidly with increasing M; the convergence decelerates when the amplitude approaches that of the steepest wave. For all examples, the maximum error was located near the wave's crest.

3.2 Gravity-capillary waves.

An iterative algorithm similar to that described above has been worked out to obtain numerical solutions of (48) with $\sigma > 0$. Here, we again assume that the surface height is an even function of x, and hence of ξ.

To describe the algorithm it is convenient to rewrite (48) in the form

$$\frac{1}{2}c_*^2 J^{-1/2} + J^{1/2}\left(\frac{\alpha}{\alpha+1}z - a_*\right) - \frac{1}{\alpha+1}J^{-1}(-x_{\xi\xi}z_\xi + z_{\xi\xi}x_\xi) = 0 \tag{58}$$

where $\alpha = 1/\sigma$; $a_\star = a\alpha/(\alpha+1)$; $c_\star^2 = c^2\alpha/(\alpha+1) = c^2/(1+\sigma)$. Note that $c_\star$ is the ratio of the actual phase velocity to the phase velocity of the linearized problem

$$c_l = \left(\frac{1}{k} + \sigma k\right)^{1/2} = \left(\frac{1}{k} + \frac{k}{\alpha}\right)^{1/2} \tag{59}$$

for wavenumber $k = 1$; the convenience of representing the results in terms of this ratio is that it does not depend on the choice of the time scale.

Table 1. Comparison of Stokes wave profiles calculated with different spectral resolutions.

s	A_{384}	$A_{96} - A_{384}$	$A_{192} - A_{384}$
0.4	0.3273	$4.2 \cdot 10^{-13}$	$1.6 \cdot 10^{-15}$
0.6	0.3986	$1.5 \cdot 10^{-6}$	$1.1 \cdot 10^{-9}$
0.8	0.4264	$8.3 \cdot 10^{-5}$	$3.2 \cdot 10^{-6}$
1.0	0.4360	$-1.4 \cdot 10^{-4}$	$-1.2 \cdot 10^{-4}$
1.2	0.4394	$-1.1 \cdot 10^{-3}$	$-1.3 \cdot 10^{-3}$
1.8	0.4405	$-5.5 \cdot 10^{-3}$	$-3.0 \cdot 10^{-3}$
2.0	0.4393	$-6.9 \cdot 10^{-3}$	$-3.9 \cdot 10^{-3}$

s	$RMSD_{96,384}$	$RMSD_{192,384}$	$MAXD_{96,384}$	$MAXD_{192,384}$
0.4	$1.3 \cdot 10^{-12}$	$1.5 \cdot 10^{-15}$	$3.7 \cdot 10^{-12}$	$2.2 \cdot 10^{-15}$
0.6	$3.9 \cdot 10^{-6}$	$3.0 \cdot 10^{-8}$	$1.7 \cdot 10^{-5}$	$1.3 \cdot 10^{-8}$
0.8	$4.8 \cdot 10^{-4}$	$3.0 \cdot 10^{-5}$	$2.3 \cdot 10^{-3}$	$1.7 \cdot 10^{-4}$
1.0	$3.0 \cdot 10^{-3}$	$6.7 \cdot 10^{-4}$	$1.1 \cdot 10^{-2}$	$3.3 \cdot 10^{-3}$
1.2	$6.8 \cdot 10^{-3}$	$2.2 \cdot 10^{-3}$	$2.1 \cdot 10^{-2}$	$9.3 \cdot 10^{-3}$
1.8	$2.1 \cdot 10^{-2}$	$7.6 \cdot 10^{-3}$	$4.9 \cdot 10^{-2}$	$2.6 \cdot 10^{-2}$
2.0	$2.6 \cdot 10^{-2}$	$9.7 \cdot 10^{-3}$	$5.9 \cdot 10^{-2}$	$3.1 \cdot 10^{-2}$

Considering the last term on the left-hand side of (58), it can be seen that

$$J^{-1}(-x_{\xi\xi} z_\xi + z_{\xi\xi} x_\xi) = Im\left(\frac{dw}{d\rho}\right) = Im(w_\xi) = (Im\ w)_\xi \tag{60}$$

where w and ρ have the same meaning as in (52). Also, if we assume that the mean of the surface height over x coordinate is zero, which is equivalent to the following choice of the 0-th Fourier coefficient:

$$\eta_0 = -\frac{1}{2} \sum_{1 \le k < M} k \eta_k^2 \ , \tag{61}$$

then parameters $a_\star$ and $c_\star$ are bound by the relationship:

$$a_\star = \frac{1}{2} c_\star^2 \ . \tag{62}$$

For pure gravity waves, this property directly follows from results by Longuet-Higgins (1975); for the general case of gravity-capillary waves, relation (61) still holds, as it can be deduced from the observation that the mean of the capillary term in (3) over x is zero.

Relations (60), (62) and (52) allow us to rewrite (58) as follows:

$$-2(\alpha+1)a_* \sinh(Re\ w) + \alpha \exp(Re\ w) z = (Im\ w)_\xi \ . \tag{63}$$

Choosing

$$S = -\frac{1}{2}(Im\ w_\xi(\xi = 0, \zeta = 0) - Im\ w_\xi(\xi = \pi, \zeta = 0)) \tag{64}$$

as the parameter determining the wave amplitude (like s in (53), it is equal to the amplitude for the linearized problem), we can now formulate the iteration scheme as follows

GC1. Assume $n = 0$, $(Im\ w)_\xi^{[0]} = -Se^\zeta \cos\xi$ (this is the solution of the linearized problem).

GC2. For given $(Im\ w)_\xi^{[n]}$, find $w^{[n]}$ in Fourier space by integration and a Hilbert transform (as in the first of equalities (41)); find $\exp(w^{[n]})$ at each gridpoint, then find $z^{[n]}$ by a Fourier transform and integration according to the second relation (52), with the integration constant defined by (61). If the maximum surface gridpoint value of $\mid z^{[n]} - z^{[n-1]} \mid$ is less than the prescribed accuracy ϵ, the iterations are completed, and $z^{[n]}$ is an approximate solution within the accuracy given.

GC3. Calculate surface values of $(Im\ w)_\xi^{[n+1]}$ as the right-hand side of (63), by substituting $w = w^{[n]}$, $z = z^{[n]}$ into the left-hand side. Similarly to step G3, $a_\star = a_\star^{[n+1]}$ must be chosen so that (64) holds for $w = w^{[n+1]}$:

$$a_*^{[n+1]} = \frac{\alpha}{2(\alpha+1)} \frac{\eta^{[n]}(0)\exp(R^{[n]}(0)) - \eta^{[n]}(\pi)\exp(R^{[n]}(\pi))}{\sinh(R^{[n]}(0)) - \sinh(R^{[n]}(\pi))} \qquad (65)$$

where

$$\eta^{[n]}(\xi) = z^{[n]}(\xi, \zeta = 0) \ , \quad R^{[n]}(\xi) = Re\ w^{[n]}(\xi, \zeta = 0) \ .$$

GC4. Find the Fourier expansion of $(Im\ w)_\xi^{[n+1]}$ by a Fourier transform; let $n = n + 1$ and return to step GC2.

Convergence of the algorithm and the dependence of wave amplitude on the parameter S for different α are characterized by Table 2. Since the wave profiles obtained for large α have two maxima, values of

$$\hat{A} = \frac{1}{2}\left(Max_{0\le j\le N}\eta(\xi = \xi^{(j)}) - Min_{0\le j\le N}\eta(\xi = \xi^{(j)})\right) \qquad (66)$$

are indicated along with A in (55). The calculations were performed with $M = 96$, $N = 432$, $\epsilon = 10^{-11}$.

For $\hat{A} = 0.4$ and $\hat{A} = 0.1$, samples of calculated wave profiles with different α are given in Figs. 2 and 3, respectively. These results were obtained with a modification of the algorithm above, which, more conveniently, uses $\hat{A}$ instead of S as a wave parameter. An important advantage of the modified version is that its domain of convergence in the $(\alpha, \hat{A})$ plane is notably larger than that of the original scheme GC1-GC4; however, computationally it is less efficient than the latter, as it requires nested calculations to numerically determine values of $a_\star$ for each iteration, while in step GC3 $a_\star$ is readily yielded by (65).

From Table 2 and Figs. 2, 3, it can be seen that with increasing α (i.e. with the capillarity coefficient σ decreasing), the wave profiles do not approach those of pure gravity waves, but rather shift their energy to smaller scales where capillarity effects are more pronounced. Beginning with $\alpha = 2$, two maxima emerge, so that $x = 0$ becomes a local minimum (the absolute minimum being always at $x = \pi$); at the same time the speed of convergence decreases rapidly, especially for small amplitudes and for those values of α which ensure equal linear phase velocities (59)) for two neighboring wavenumbers k, $k + 1$, namely $\alpha = 2$ $(k = 1)$ and

$\alpha = 6$ $(k = 2)$.

Table 2. Amplitudes and numbers of iterations N_{it} for gravity-capillary waves calculated with different α and S. Blank entries mean that the scheme failed to converge.

	S	0.001	0.1	0.2	0.4	0.6	0.8	1
α								
	A	0.001000	0.1000	0.2000	0.4000	0.6000	0.8000	1.0000
0	$\hat{A}$	0.001000	0.1000	0.2000	0.4000	0.6000	0.8000	1.0000
	N_{it}	4	16	18	20	21	21	20
	A	0.001000	0.0996	0.1969	0.3772	0.5315	0.6583	0.7606
0.5	$\hat{A}$	0.001000	0.0996	0.1969	0.3772	0.5315	0.6583	0.7606
	N_{it}	22	41	41	39	39	43	43
	A	0.001000	0.0971	0.1814	0.3109	0.4066	0.4815	0.5420
1	$\hat{A}$	0.001000	0.0971	0.1814	0.3109	0.4066	0.4815	0.5420
	N_{it}	37	61	48	47	44	43	42
	A	0.001000	0.0880	0.1497	0.2382	0.3050	0.3593	0.4049
1.5	$\hat{A}$	0.001000	0.0880	0.1497	0.2382	0.3050	0.3593	0.4049
	N_{it}	79	93	58	48	43	41	39
	A	0.000991	0.0655	0.1090	0.1760	0.2291	0.2738	
2	$\hat{A}$	0.001114	0.0711	0.1165	0.1844	0.2375	0.2819	
	N_{it}	7966	157	81	44	41	40	
	A	0.000264	0.0262	0.0512	0.0967	0.1361		
3	$\hat{A}$	0.074839	0.0895	0.1064	0.1417	0.1750		
	N_{it}	152	106	88	62	54		
	A	0.000162	0.0162	0.0323	0.0636			
4	$\hat{A}$	0.076547	0.0853	0.0955	0.1182			
	N_{it}	161	134	122	97			
	A	0.000124	0.0124	0.0247	0.0490			
5	$\hat{A}$	0.058195	0.0653	0.0742	0.0946			
	N_{it}	212	178	157	138			
	A	0.000111	0.0109					
6	$\hat{A}$	0.000324	0.0247					
	N_{it}	2771779	2051					

Neither the scheme GC1-GC4 nor its aforementioned modification converged with $\alpha > 6$; however, the modified scheme converged for $\hat{A}$

values considerably larger than those indicated in Table 2.

The dependence of the normalized phase velocity c_* on $\sigma = 1/\alpha$, as illustrated by Fig. 4, is consistent with the behavior of the corresponding profiles. When σ decreases but remains positive, c_* decreases and does not approach its value at sigma=0. The latter is always greater than 1 and, except for a small interval in the vicinity of the maximum $\hat{A}$, is an increasing function of $\hat{A}$, while for $\sigma \neq 0$ the calculated c_* is a decreasing function of $\hat{A}$ and always less than 1. In fact, for small values of $\hat{A}$, the phase velocity corresponding to a given σ turns out to be close to the minimum value of c_l over k in (59).

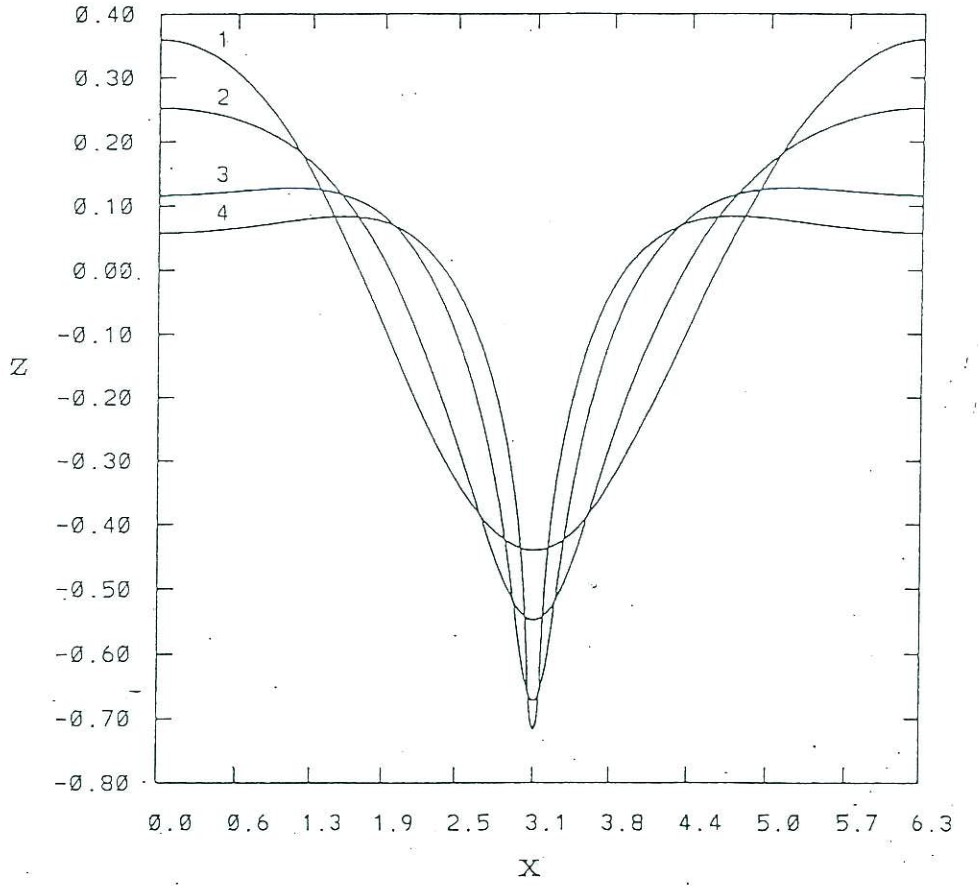

Figure 2: Profiles of gravity-capillary waves, $\hat{A} = 0.4$. Curve 1 - $\alpha = 0$ (Crapper's wave), 2 - $\alpha = 1$, 3 - $\alpha = 2$, 4 - $\alpha = 3$.

For most cases represented in Table 2, a comparison was performed

with results obtained for a higher resolution ($M = 384$, $N = 1728$). The maximum difference between surface profiles as defined in (56) never exceeded $1.2 \cdot 10^{-11}$, which means that the truncation errors are negligible.

3.3 Pure capillary waves.

For pure capillary waves, which are described by (58) if we formally set $\alpha = 0$, the solution is represented by a simple formula (Crapper, 1957).

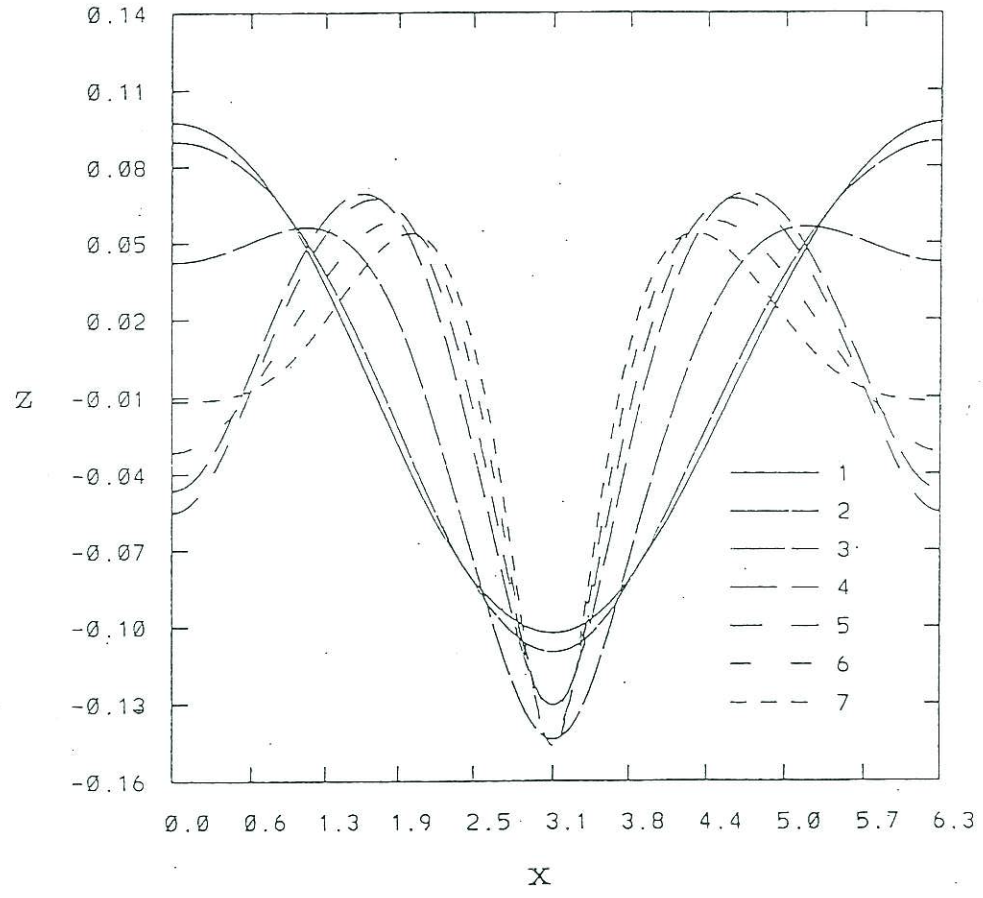

Figure 3: Profiles of gravity-capillary waves, $\hat{A} = 0.1$. Curve 1 - $\alpha = 0$ (Crapper's wave), 2 - $\alpha = 1$, 3 - $\alpha = 2$, 4 - $\alpha = 3$, 5 - $\alpha = 4$, 6 - $\alpha = 5$, 7 - $\alpha = 6$.

In our notation, it can be written as

$$x(\xi, \zeta) = \xi + \frac{4q \sin \xi}{1 - 2q \cos \xi + q^2} \quad , \tag{67}$$

$$z(\xi,\zeta) = \zeta + \frac{4q(\cos\xi - q)}{1 - 2q\cos\xi + q^2} - \frac{1}{2}A^2 \quad , \tag{68}$$

where

$$q = be^{\zeta} \quad , \quad b = \frac{-2 + \sqrt{4 + A^2}}{A} \quad , \tag{69}$$

and A , $\hat{A}$, S, b, c_*, a_* are bound by the following relationships:

$$A = \hat{A} = S = \frac{4b}{1 - b^2} \quad , \quad \frac{1}{2}c_*^2 = a_* = \frac{1}{\sqrt{4 + A^2}} \quad . \tag{70}$$

The last term in (68) may be any constant but here it is chosen to satisfy condition (62).

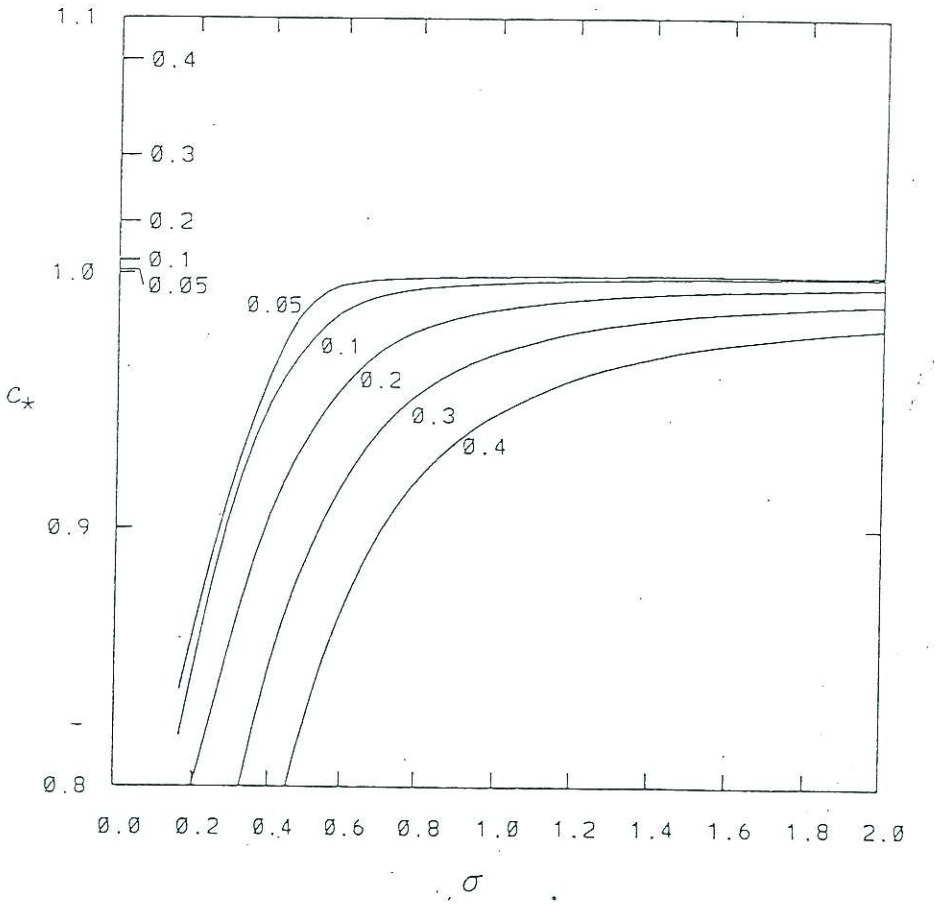

Figure 4: Normalized phase velocity $c_* = c/\sqrt{1+\sigma}$ as a function of nondimensional capillarity coefficient σ. Wave amplitudes A are indicated at the respective curves.

Exact solution (67)-(70) was used as another means to validate scheme GC1-GC4 with $\alpha = 0$. For all tested amplitudes, up to the maximum possible amplitude (e.g. Crapper, 1984), the maximum difference between the numerical ($M = 96$) and the exact solutions as defined in (56) was less than $5 \cdot 10^{-12}$.

4. Solution of the nonstationary equations

For spatial approximation of system (42), (43) we use a Galerkin-type (or "spectral") method based on Fourier expansion of the prognostic variables with a finite truncation number M. The system is thus reduced to that of ordinary differential equations for $4M + 2$ Fourier coefficients $\eta_k(\tau)$, $\phi_k(\tau)$, $-M \leq k \leq M$:

$$\dot{\eta}_k = E_k(\eta_{-M}, \eta_{-M-1}, ..., \eta_M, \phi_{-M}, \phi_{-M-1}, ..., \phi_M) \tag{71}$$

$$\dot{\phi}_k = F_k(\eta_{-M}, \eta_{-M-1}, ..., \eta_M, \phi_{-M}, \phi_{-M-1}, ..., \phi_M) \tag{72}$$

where E_k, F_k are, respectively, the Fourier expansion coefficients for the right-hand sides of (42) and (43) as functions of ξ.

To calculate E_k, F_k as functions of the prognostic variables η_k, ϕ_k, formulas (23) - (28) are used for the spatial derivatives (which are thus evaluated exactly), and the nonlinearities are calculated with the so-called transform method (Orszag, 1970; Eliassen, 1970), i.e., by their evaluation on a spatial grid. If $Y(u(\xi), v(\xi), w(\xi), ...)$ is a nonlinear function of its arguments which are represented by their Fourier expansions, gridpoint values $u(\xi^{(j)})$, $v(\xi^{(j)})$, $w(\xi^{(j)})$,... are first calculated, i.e., inverse Fourier transforms are performed; then $Y^{(j)} = Y(u(\xi^{(j)}), v(\xi^{(j)}), w(\xi^{(j)}), ...)$ are evaluated at each gridpoint; finally, the Fourier coefficients Y_k of the function Y are found by direct Fourier transform. Here $\xi^{(j)} = 2\pi(j-1)/N$, and N is the number of gridpoints.

For the method to be a purely Galerkin one, i.e., to ensure the minimum mean square approximation error, the Fourier coefficients E_k, F_k need to be evaluated exactly for $-M \leq k \leq M$. For this purpose, we must choose

$$N > (\nu + 1)M \tag{73}$$

where ν is the maximum order of nonlinearities. Since the right-hand sides of (42), (43) include division by the Jacobian, the nonlinearity is of infinite order so that, strictly, the above condition on N cannot be met. However, numerical integrations show that if we choose a value of N ensuring exact evaluation of the cubic nonlinearities ($\nu = 3$ in (73)), a further increase in N (with fixed M) virtually does not impact the numerical solution. For most runs, $M = 96$ and $N = 432$ were used.

However high the spectral resolution might be, for long-term integrations one must parameterize the energy flux into the severed part of the spectrum ($k > M$); otherwise, spurious energy accumulation at large wave numbers will corrupt the numerical solution. Simple dissipation terms were added to the right-hand sides of equations (71), (72) for this purpose:

$$\dot{\eta}_k = E_k - \mu_k \eta_k \ , \tag{74}$$

$$\dot{\phi}_k = F_k - \mu_k \phi_k \ ; \tag{75}$$

with

$$\mu_k = \begin{cases} rM \left(\frac{|k| - k_d}{M - k_d} \right)^2 & \text{if } | \, k \, | > k_d \\ 0 & \text{otherwise} \end{cases} \tag{76}$$

where $k_d = M/2$ and $r = 0.25$ were chosen for most runs; the sensitivity of the results to reasonable variations of k_d and r was low. The dissipation effectively absorbs the energy at wave numbers close to the truncation number M while leaving longer waves virtually intact (note that wave numbers $-k_d \leq k \leq k_d$ are not affected).

For time integration, the fourth-order Runge-Kutta scheme was used.

5. Validation of the model

The stationary solutions dealt with in Section 3 were used for validation of the nonstationary model (equations (42), (43)). In the model's coordinate system bound to the mean flow, progressive waves were simulated starting from initial conditions calculated as stationary solutions in a moving (bound to the phase of the wave) coordinate system. If such a wave is stable with respect to truncation errors, it should propagate with

its specific phase velocity without changes of shape. The model was validated for three types of waves (experiments 1-3 in Table 3, respectively); pure capillary waves described analytically by (67)-(70) (Crapper, 1957); pure gravity (Stokes) waves; and gravity-capillary waves obtained numerically as described in section 3 (experiments 1-3 in Table 3).

Table 3. List of numerical experiments (G - pure gravity waves; C - pure capillary waves; GC - gravity-capillary waves; A - amplitude of stationary wave (55); PS - power spectrum (83) with parameters k_0 , A_0 ; RP - random phases; a_k - amplitude of k-th Fourier component of surface height. The last column indicates nonzero Fourier components of the initial conditions, in ξ-coordinate).

No.	*Type*	*Initial conditions*	*Modes*
1	C	*Crapper's wave*, $A = 0.7$	*All*
2	G	*Stokes wave*, $A = 0.3$	*All*
3	$GC, \sigma = 0.04$	*Stationary GC wave*, $A = 0.3$	*All*
4	$GC, \sigma = 0.05$	*PS, RP*, $k_0 = 1$, $A_0 = 0.1$	$1 - 25$
5	G	*Lake & Yuen waves*, $a_3 = a_5 = 0.04$	$3, 5$
6	G	*White noise*, $a_k = 0.001$	$1 - 25$
7	G	*PS, RP*, $k_0 = 10$, $A_0 = 0.01$	$1 - 25$
8	$GC, \sigma = 0.005$	*PS, RP*, $k_0 = 10$, $A_0 = 0.01$	$1 - 25$
9	C	*PS, RP*, $k_0 = 10$, $A_0 = 0.01$	$1 - 25$
10	G	*Stokes wave*, $A = 0.3$,	*All+*
		+ white noise, $a_k = 0.001$	$15 - 39$

Integration of equations (45), (46) for Crapper's waves ($\alpha = 0$) was performed for the value of $A = 0.7$ up to $\tau = 100$, i.e. for about 16 periods of the wave, with the time step $\Delta\tau = 0.001$. Stokes waves ($\sigma = 0$) and gravity-capillary waves ($\alpha = 0.04$) were simulated for $A = 0.3$ up to $\tau = 1000$ (~ 160 periods) with $\Delta\tau = 0.01$. Visual comparison of instantaneous wave profiles (not shown) obtained for different values of τ during the simulations showed that in all cases the surfaces moved without any visible disturbances. To estimate "steadiness" of the numerical solution quantitatively, we calculated the phase velocities and amplitudes of the Fourier components for consecutive values of τ with intervals of $8\Delta\tau$ and obtained their temporal means and standard deviations over the period of integration (Table 4).

The instantaneous phase velocity of the k-th wave component may be calculated as follows

$$C(k) = \dot{\lambda}_k = \frac{\eta_{-k}\dot{\eta}_k - \eta_k\dot{\eta}_{-k}}{k(\eta_k^2 + \eta_{-k}^2)}, \tag{77}$$

where η_k are the Fourier expansion coefficients of the surface as defined by (11), and λ_k are the phases:

$$\eta(\xi,\tau) = \sum_{0\le k\le M} \sqrt{\eta_k^2 + \eta_{-k}^2}\cos\left(k(\xi - \lambda(\tau))\right) \quad .$$

If there is only one wavenumber-frequency spectrum component corresponding to wave number k, i.e. if each Fourier component of the surface propagates with a single phase velocity, formula (77) yields a constant value of C for each k. In our case of progressive waves retaining their shapes, this value is the same for all k. For arbitrary wave fields, there may be many modes (wavenumber-frequency spectrum components) which have the same wave number but propagate with different phase speed due to nonlinear effects, and even in the case of linear waves there are, generally, two k-th modes propagating in opposite directions with the same absolute speed. In such cases, (77) yields a weighed average phase velocity of the modes, which generally vary in time. In the described runs, modes moving in the opposite direction were generated during the integration because of truncation errors. The amplitudes of these modes were by several orders of magnitude smaller than those of the "true" (positively directed) components of the simulated waves, but they manifest themselves in small shifts and perturbations of the instantaneous phase velocities, whose temporal means and standard deviations are given in Table 4 for the first 15 modes.

The calculated phase velocities are very close to their values obtained for the stationary solutions (also given in Table 4); although they slightly decrease with increasing the wave number, their mean errors and standard deviations are small for all the three types of waves. Since conservation of the amplitudes (not shown) was also very accurate (the deviations of their values during the simulations from their initial values were always less than 10^{-7} for the Stokes wave and less than 10^{-11} for the capillary and gravity-capillary waves), the modes retained their initial energies and remained consistent in phase; consequently, the simulated waves did

not noticeably change their shapes during the integration. This result implies that these waves are stable with respect to truncation errors, and that the numerical solutions yielded by the model approximate the solutions of the original differential equations with high accuracy.

Table 4. Themporal means and standard deviations of the phase velocities for the first 15 modes of Crapper's, Stokes and gravity-capillary progressive waves. (C is the "exact" phase velocity, i.e. that obtained for the stationary solution).

	Crapper's waves	*Stokes waves*	*CG waves*
	$A = 0.7,\ C = 0.971524$	$A = 0.3,\ C = 1.046040$	$A = 0.3,\ C = 1.160514$
1	$0.971524\ (1 \cdot 10^{-5})$	$1.045997\ (2 \cdot 10^{-5})$	$1.160514\ (2 \cdot 10^{-5})$
2	$0.971523\ (1 \cdot 10^{-5})$	$1.045940\ (2 \cdot 10^{-5})$	$1.160513\ (2 \cdot 10^{-5})$
3	$0.971522\ (1 \cdot 10^{-5})$	$1.045844\ (2 \cdot 10^{-5})$	$1.160512\ (2 \cdot 10^{-5})$
4	$0.971521\ (1 \cdot 10^{-5})$	$1.045711\ (2 \cdot 10^{-5})$	$1.160510\ (2 \cdot 10^{-5})$
5	$0.971520\ (1 \cdot 10^{-5})$	$1.045539\ (2 \cdot 10^{-5})$	$1.160507\ (2 \cdot 10^{-5})$
6	$0.971518\ (1 \cdot 10^{-5})$	$1.045329\ (2 \cdot 10^{-5})$	$1.160505\ (2 \cdot 10^{-5})$
7	$0.971516\ (1 \cdot 10^{-5})$	$1.045081\ (2 \cdot 10^{-5})$	$1.160501\ (2 \cdot 10^{-5})$
8	$0.971514\ (1 \cdot 10^{-5})$	$1.044790\ (2 \cdot 10^{-5})$	$1.160497\ (2 \cdot 10^{-5})$
9	$0.971511\ (1 \cdot 10^{-5})$	$1.044472\ (2 \cdot 10^{-5})$	$1.160493\ (2 \cdot 10^{-5})$
10	$0.971508\ (1 \cdot 10^{-5})$	$1.044410\ (2 \cdot 10^{-5})$	$1.160488\ (2 \cdot 10^{-5})$
11	$0.971505\ (1 \cdot 10^{-5})$	$1.043709\ (2 \cdot 10^{-5})$	$1.160482\ (2 \cdot 10^{-5})$
12	$0.971502\ (1 \cdot 10^{-5})$	$1.043271\ (2 \cdot 10^{-5})$	$1.160476\ (2 \cdot 10^{-5})$
13	$0.971500\ (1 \cdot 10^{-5})$	$1.042795\ (2 \cdot 10^{-5})$	$1.160470\ (2 \cdot 10^{-5})$
14	$0.971494\ (4 \cdot 10^{-5})$	$1.042281\ (2 \cdot 10^{-5})$	$1.160463\ (2 \cdot 10^{-5})$
15	$0.971489\ (2 \cdot 10^{-4})$	$1.041730\ (2 \cdot 10^{-5})$	$1.160456\ (2 \cdot 10^{-5})$

Another criterion of model accuracy is conservation of the integral invariants during the integration, i.e. of volume

$$V = (2\pi)^{-1} \int_0^{2\pi} z x_\xi d\xi \ , \tag{78}$$

horizontal momentum

$$I = (2\pi)^{-1} \int_0^{2\pi} \phi z_\xi d\xi \ , \tag{79}$$

and energy $E = E_K + E_{PG} + E_{PT}$, where

$$E_K = (2\pi)^{-1} \int_0^{2\pi} \phi\phi_\zeta d\xi \tag{80}$$

is the kinetic energy,

$$E_{PG} = (2\pi)^{-1} \int_0^{2\pi} z^2 x_\xi d\xi \tag{81}$$

is the potential energy of gravity, and

$$E_{PT} = (2\pi)^{-1}\sigma \int_0^{2\pi} (J^{-1/2} - 1) d\xi \tag{82}$$

is the potential energy of surface tension. Formulas (78) - (82) are obtained by transformation of starndard Cartesian-coordinate expressions for the invariants into (ξ, ζ) coordinates and refer to a unit length along the horizontal axis.

An example of the temporal evolution of E_K, E_P, E_T, and E is represented in Fig. 5 for the case of gravity-capillary waves with $\sigma = 0.05$. The initial surface was chosen in the form of a superposition of $M_m = 25$ linear modes with amplitudes a_k assigned according to

$$a_k = \begin{cases} A_0 \left(\frac{k}{k_0}\right)^P & k_0 \le k \le k_0 + M_m - 1 \\ 0 & \text{otherwise} \end{cases} \tag{83}$$

where $A_0 = a_{k_0}$ is the amplitude of the k_0-th mode, and power $P < 0$ is the amplitude decrement. The Fourier coefficients were calculated as

$$\eta_k = a_k \begin{cases} \sin\lambda_k & k \le 0 \\ \cos\lambda_k & k > 0 \end{cases} \tag{84}$$

where the λ_k are random phases.

The Fourier coefficients for the initial surface velocity potential Φ were assigned so that, in linear approximation, all wave components propagated in the positive direction. It can be easily derived from the linear theory that this is ensured by the relations:

$$\phi_k = b_k \eta_{-k}, \quad b_k = sign(k)\sqrt{\frac{1+\sigma k^2}{k\tanh(kH)}} \ . \tag{85}$$

For the calculations represented in Fig. 5, $\sigma = 0.05$, $A_0 = 0.1$, $P = -\frac{3}{2}$, $k_0 = 1$, $M_m = 25$, and $H = \infty$ (deep water). The horizontal

momentum I and the volume V conserved with relative error margins of the order of 10^{-13} and 10^{-11} respectively. From Fig. 5 it can be seen that while the energy components E_K, E_{PG}, and E_{PT} show significant fluctuations, their sum nearly conserves; its slow decrease is due to damping at high wave numbers. Similar results were obtained for a number of other test simulations, including ones with a finite depth H.

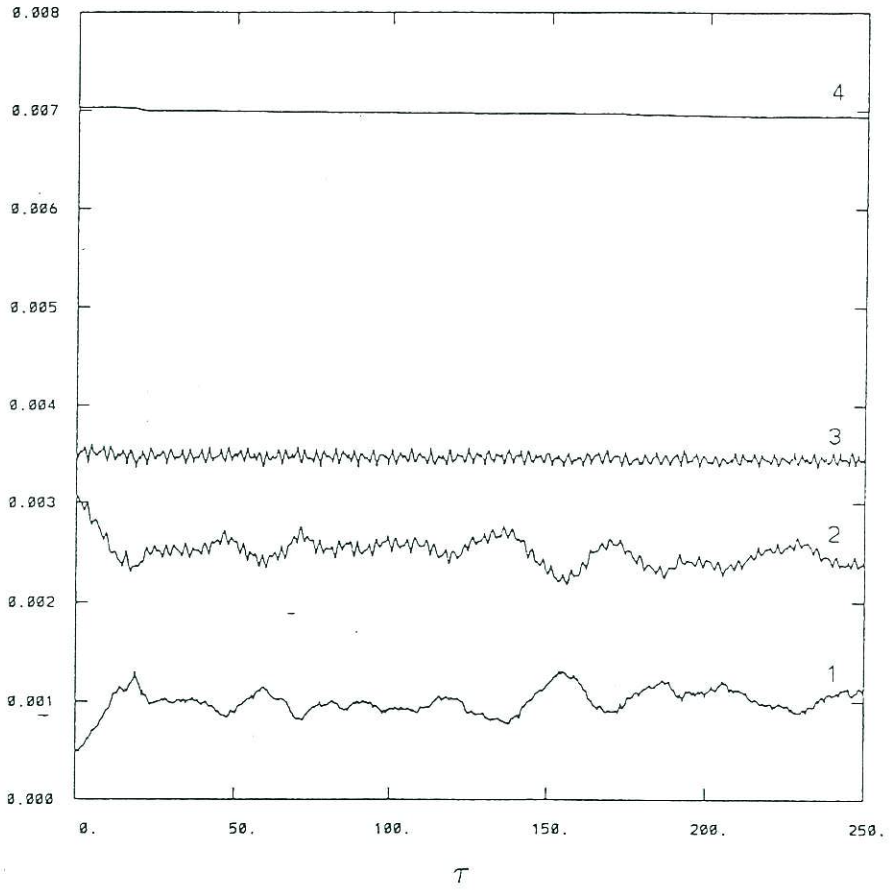

Figure 5: Time evolution of gravitational potential energy E_{PG} (curve 1), kinetic energy E_K (2), potential energy of surface tension E_{PT} (3) and their sum E (4) (Exp. 4) for gravity-capillary waves ($\sigma = 0.04$).

The results described in this section suggest that the model can successfully simulate evolution of multi-component wave fields.

6. Results of the simulations

The progressive gravity, capillary, and gravity-capillary waves dealt with in sections 3 and 5 represent a very special case of nonlinear interactions; they consist of Fourier modes which, rather than obey the linear dispersion relation (59), propagate with one and the same phase speed. It is evident that similar effects may also be observed in more general situations: due to the impact of nonlinearity, a multi-mode wave motion cannot be represented as a superposition of Fourier modes propagating with their linear phase speeds; moreover, a specific wave number, generally, is not associated with any single phase speed. Perhaps the most striking manifestation of nonlinearity is that some shorter waves propagate with phase speeds close to that of long waves. The existence of such forced (or "bound") components was clearly demonstrated in many laboratory and observational studies (Yuen and Lake, 1982). Various explanations has been proposed for this phenomenon, including wind-wave and wave-current coupling, but Lake and Yuen (1978) found that this effect is mainly due to nonlinearity of the waves themselves. Realistic wave fields contain both types of waves, free and bound, for the same wave number, and the "observed" phase velocities reflect a combined effect of the two. Partitioning of the energy between these types of waves depends on the wave spectrum, whose shape is influenced by external forcing. A theoretical explanation of this effect based on Zakharov's (1968) equation was proposed by Yuen and Lake (1982). The phenomenon was reproduced in a 1-D hydrodynamical potential wave model by Chalikov and Liberman (1991) who pointed out that, with phase velocities calculated according to (77), each Fourier component turns out to have a phase speed value much greater than that predicted by the linear theory. They also found that the phase velocity varies in time, and that its standard deviation increases with the wave number. However, their model could not perform long-term simulations with high spectral resolution, which require a greater computational efficiency and accuracy. Experience with the new model described above has shown that, for analysis of wavenumber-frequency spectra to be virtually unaffected by further increase in the model resolution and the length of simulations, it is essential that the model be run for several hundred periods of the longest wave with the spectral truncation number M of the order of 100. In the runs discussed below, $M = 96$ and $N = 432$ was used.

We will first consider the results of a model simulation (Exp. 5) of one of the experiments by Lake and Yuen (1978) who investigated the

nonlinear interaction of two gravity waves with wave numbers close to each other. They evaluated the phase velocities of different modes by calculating the coherence of the surface elevation values in two sections of a wave channel (Fig. 8 of Lake and Yuen (1978)), and found out that the phase velocities of the waves not produced by the wave maker were close to those of the primary waves. It is hardly possible to exactly reproduce their experiment in a model simulation, since the amplitudes of the waves were not reported, and there are uncertainties as to modeling of the forcing. In the model, to obtain a flow qualitatively similar to that in their experiment, we used a superposition of the 3rd and the 5th waves with equal amlitudes of 0.04 as the initial conditions for the surface elevation; no forcing was imposed. In this and all other runs (except those dealing with progressive waves described in section 3), the initial conditions for the velocity potential on the surface were prescribed according to the linear theory for unidirectional waves (formula (85)). The simulation was performed with $\Delta\tau = 0.01$ up to $\tau = 1000$.

The wavenumber spectra (calculated from Fourier expansions of the surface elevation with respect to x coordinate) averaged for 6 consecutive time intervals (167 nondimensional time units each) are given in Fig. 6. The energy decreases slowly in time because of dissipation at high wave numbers. The energy of the 3rd mode is nearly conserved but the energy of the 5th mode (which was initially equal to that of the 3rd mode) is considerably less.

In Fig. 7, temporal means and standard deviations of the instantaneous phase velocities (77) are shown. It is seen that the linear dispersion relation is observed only for wave numbers $2 \leq k \leq 5$. For $k > 5$, the waves propagate significantly faster than the linear waves but slower than the primary waves. This effect is clearly pronounced only for the temporal means of the phase velocities; the instantaneous values vary highly (as pointed out in Chalikov and Liberman, 1991), which is reflected by large standard deviations for wave numbers $k > 5$. This scattering is caused by the presence of both bound and free waves.

More information on free and bound waves and their phase velocities is provided by the wavenumber-frequency spectrum $S(k,\omega)$ whose logarithm is shown in Fig. 8 along with the logarithms of the time-averaged wavenumber ($S^k(k)$) and frequency ($S^\omega(\omega)$) spectra. The picture of S

looks as if it consisted of patches; this effect is caused by the high density of the contour lines. To calculate S for each k, instantaneous Fourier expansions with respect to x coordinate were stored during the entire period of integration $0 \leq \tau \leq 1000$ with time intervals of 0.08, and Fourier transforms with respect to time were used. In this and other runs, the length of simulation ensured sufficient frequency resolution (here, $\delta\omega = 2\pi/1000$) which is essential for the analysis of the spectra, and the maximum resolved frequency ($\omega = \pi/0.08$ for this run) far exceeded any possible "physical" value of ω and thus rendered the transforms' aliasing error negligible.

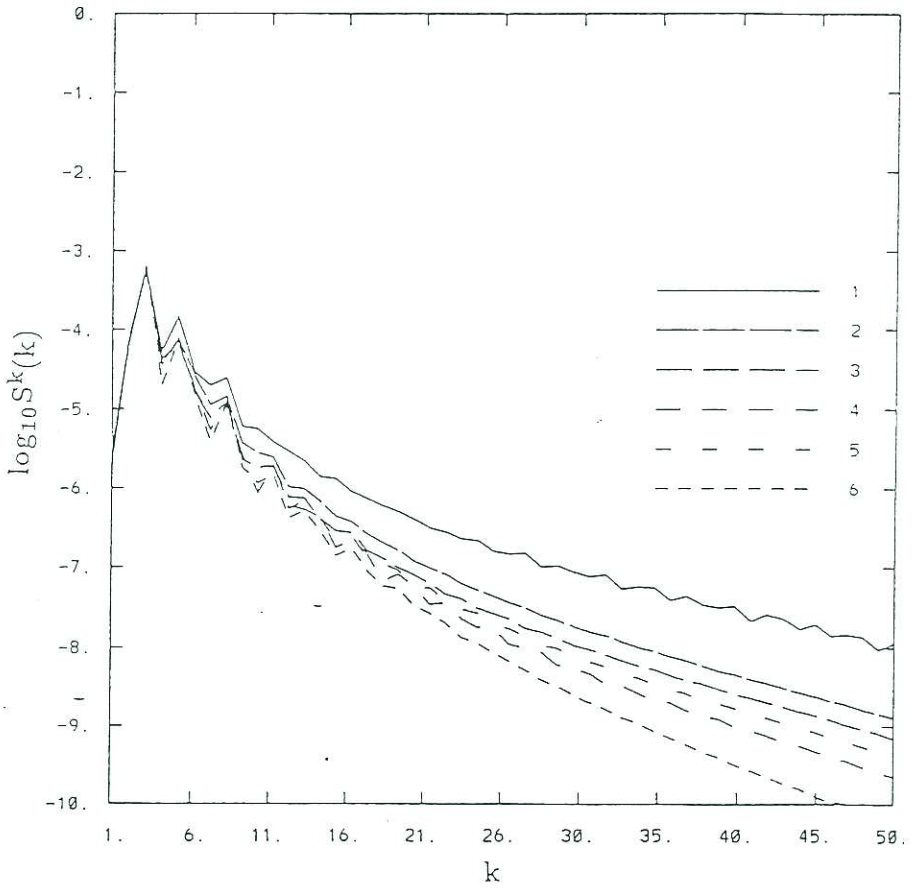

Figure 6: Time-averaged wavenumber spectra $S^k(k)$ for 6 consecutive time intervals of length $\delta\tau = 167$, Exp. 5.

The most remarkable feature of the wavenumber-frequency spectrum is that it is split into a set of branches in a regular way. This effect is well pronounced for the waves propagating in the direction prescribed

originally by using (85) ($k > 0$ in Fig. 8), but it is also noticeable for the waves moving in the opposite direction, which were not present in the initial conditions ($k < 0$ in Fig. 8 where the sign of k is determined by the sign of the component's phase velocity, while ω is assumed positive). A considerable part of energy is borne by the components which nearly obey the linear dispersion relation $\omega^2 = \mid k \mid$ (Curve 1).

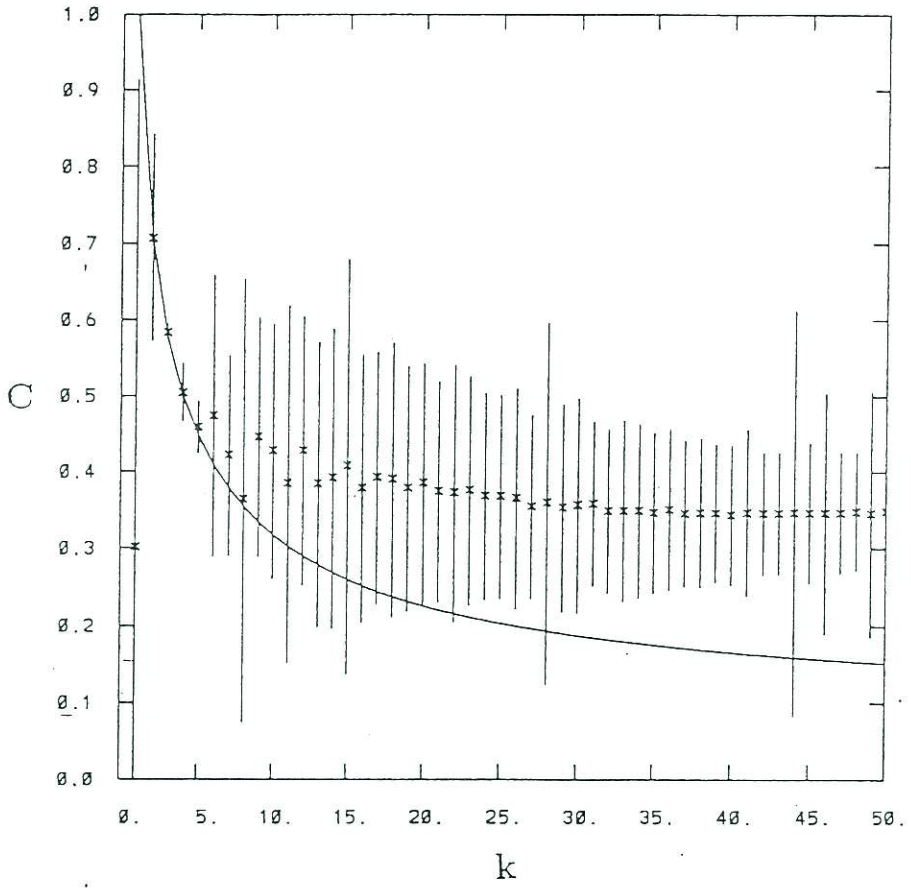

Figure 7: Time-averaged phase velocity (77) (asterics) and its standard deviation (vertical bars) as functions of wave number k, Exp. 5 (simulation of the non-wind experiment by Lake and Yuen, 1978). The curve corresponds to the linear dispersion relation.

The remaining energy mostly belongs to what may be, with some generalization, interpreted as bound components, which propagate with the phase velocities of their carrying waves from near Curve 1 and lie on the branches approximated by the curves

$$\omega^2 = n \mid k \mid \ , \qquad (86)$$

where n (the number of the branch) is a positive integer. (Strictly, not all of the components (86) with $n > 1$ may be called bound, since those with k which is not a multiple of n have no "carrier". However, they propagate as if they were bound to a free wave with wave number k/n).

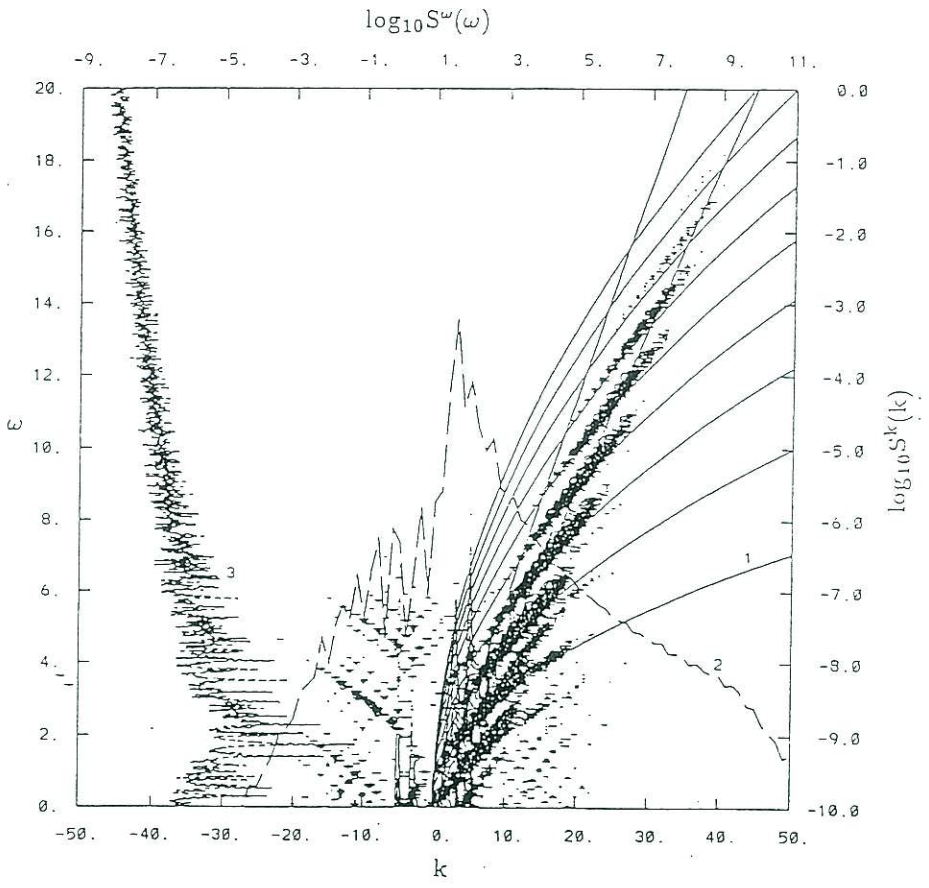

Figure 8: Time-averaged spectral characteristics for the period of $\delta\tau = 1000$, Exp. 5. Curve 1 - linear dispersion relation $\omega^2 = k$, the other parabolas - $\omega^2 = nk$, $k = 1, 2, ..., 9$. The contour lines of $\log_{10} S(k, \omega)$ (wavenumber-frequency spectrum) are seen as concatenated in patches. Curve 2 is $\log_{10} S^k(k)$ (wavenumber spectrum, right scale), Curve 3 is $\log_{10} S^\omega(\omega)$ (frequency spectrum, top scale).

Each of the branches follows relation (86) closely at lower wave numbers k and tends to straighten at higher wave numbers so that, with k increasing, the group velocity appears to tend to a constant whose value

is the same for all the branches. Along with this set of branches, there are also other patterns which, despite their relatively low energy, show a notably regular discrete structure.

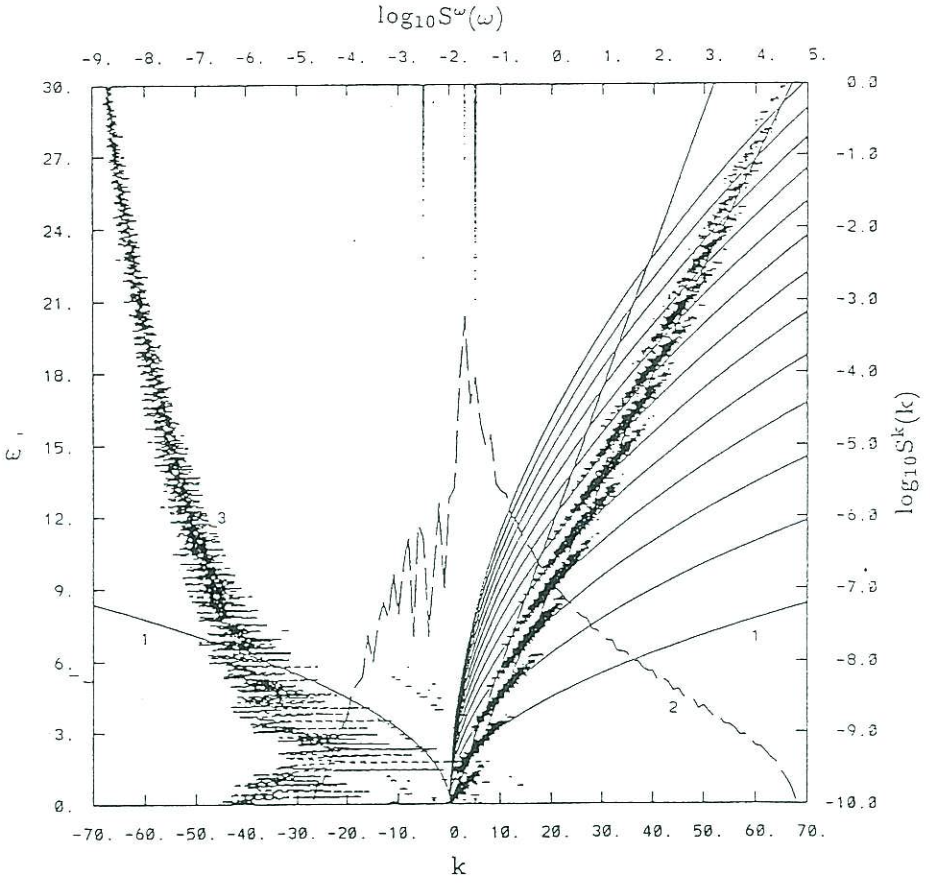

Figure 9: Same as in Fig. 8, but instead of $\log_{10} S$ the contours of normalized spectrum $S(k,\omega)/S^{\omega}(\omega)$ are plotted.

Another representation of the wavenumber-frequency spectrum can be obtained through normalizing each value of $S(k,\omega)$ by $S^{k}(k)$ (which for a given k is the spectral density integrated over ω). The normalized spectrum (Fig. 9), which characterizes the fractional energy distribution over frequencies for each wave number, exhibits up to 13 branches of the type described above. A most peculiar feature of the spectrum, clearly seen in both Fig. 8 and 9, is a pattern which may be approximated by a straight line passing through the origin of the coordinates; the corresponding modes thus tend to propagate with roughly the same phase

velocity which seems to be equal to the aforementioned apparent limit value of group velocity.

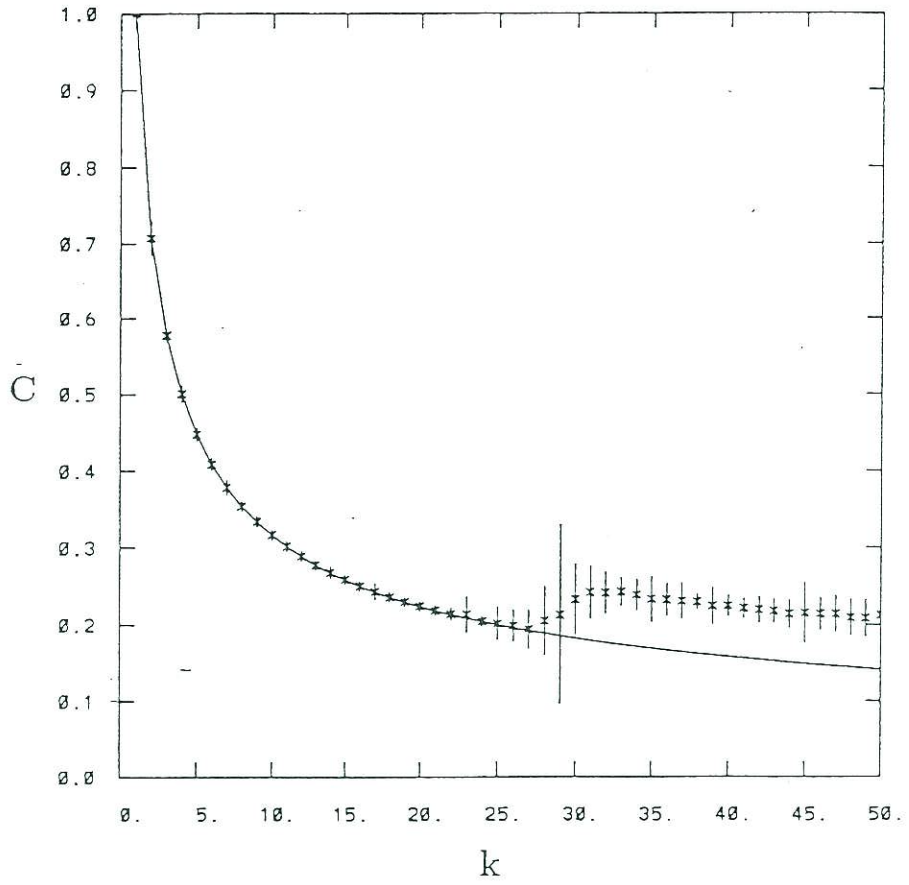

Figure 10: Same as in Fig. 7 but for Exp. 6 (initial conditions approximating white noise).

The next numerical experiment (Exp. 6) simulated a pure gravity wave field with initial conditions approximating white noise; other features were the same as in Exp. 5. For the first 25 wave numbers k, the initial amplitudes were assigned the same value of 0.001, with random phases; for $k > 25$, the amplitudes were set to zero. The phase velocities (77) and their standard deviations are shown in Fig. 10. Because the amplitudes of the initially assigned waves were small, these waves nearly obey the linear theory: their phase velocities are close to the linear ones and have small standard deviations. The waves produced by the nonlinear interactions ($k > 25$) again propagate faster than linear

waves. In the wavenumber-frequency spectrum (Fig. 11), only the first two ($n = 1$, where most of the energy is concentrated, and $n = 2$) of the "main branches" approximated by (86) are seen. The remaining part of the energy is small, and, again, most of it is concentrated near a straight line passing through the origin, while the remainder is distributed along other regularly located curves. Further investigations are needed for explanation of these features.

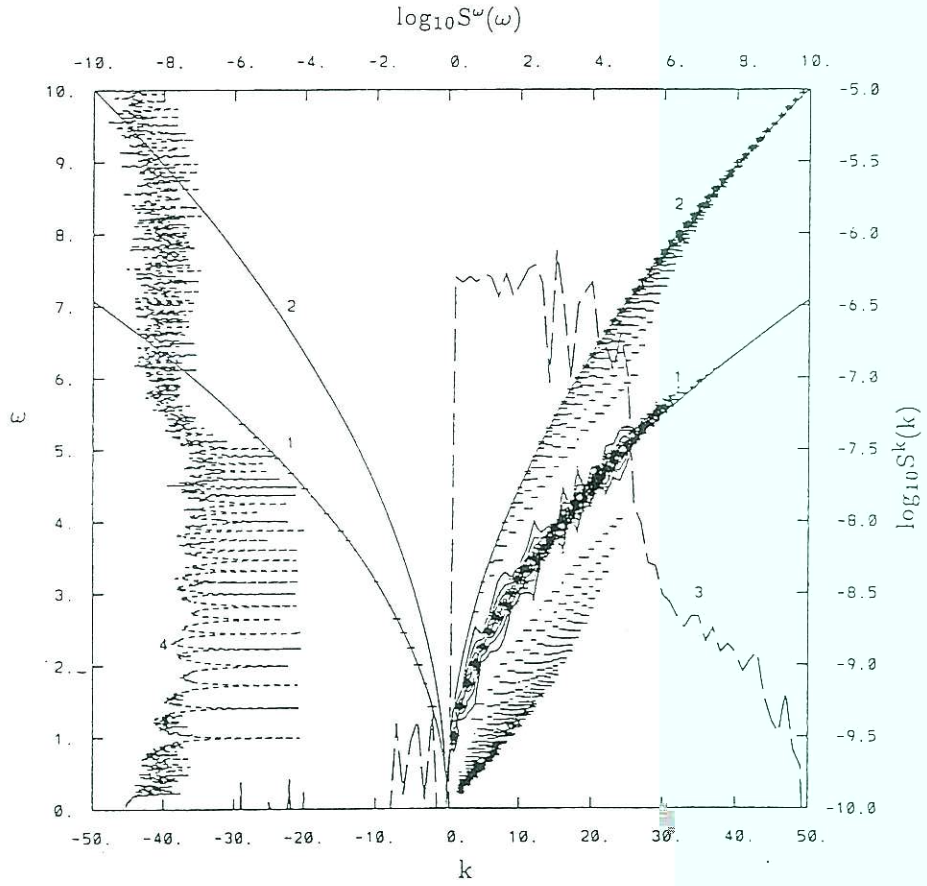

Figure 11: Same spectral characteristics as in Fig. 8 but for "white noise" simulation (Exp. 6). Curves 1 and 2 are dispersion relation $\omega^2 = nk$ ($n = 1,\ 2$), 3 - $S^k(k)$, 4 - $S^\omega(\omega)$.

Another run (Exp. 7), which also differed from the previously described ones by the initial amplitudes only, was designed to approximate a real ocean wave field. The initial spectrum of the surface elevation was prescribed by (83), (84), with $A_0 = 0.01$, $k_0 = 5$, $P = -1.5$. The results

are shown in Fig. 12. In the wavenumber-frequency spectrum, we again see most of the energy concentrated along the "main" branches (86), and the "quasi-rectilinear" branch is again quite distinct.

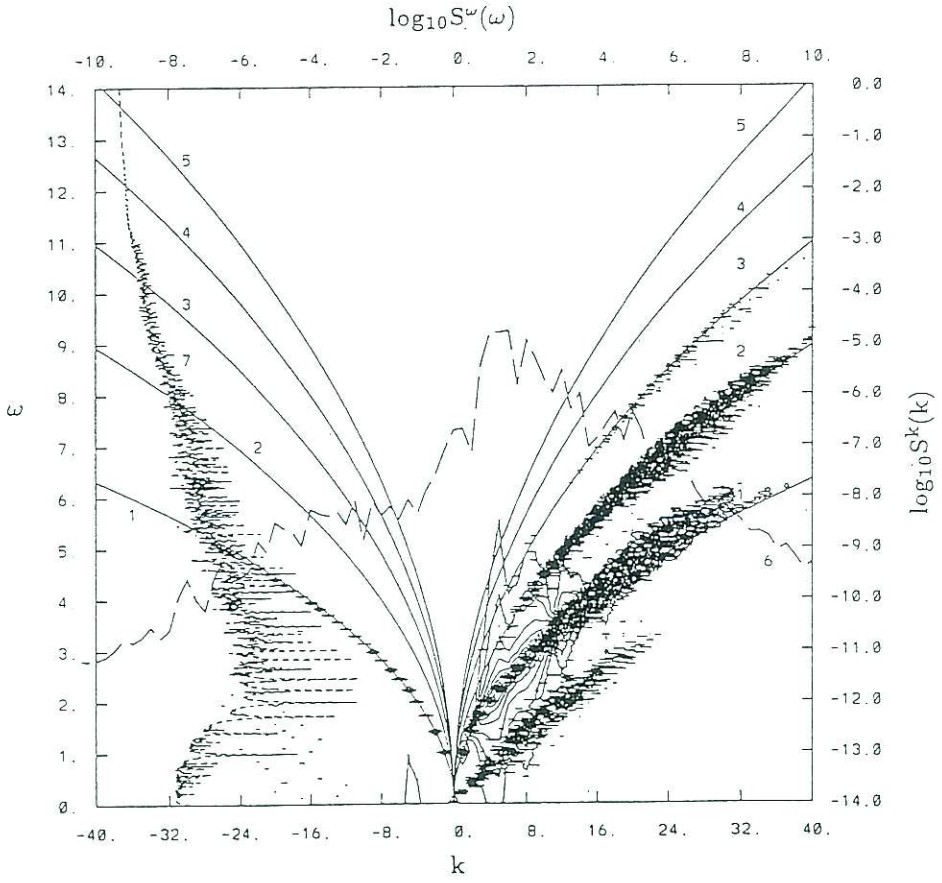

Figure 12: Same spectral characteristics as in Fig. 8 but for Exp. 7 (initial conditions with spectrum (83) approximating real waves)

In the next run (Exp. 8), gravity-capillary waves were simulated, with the nondimensional capillarity coefficient $\sigma = 0.05$. The initial conditions were chosen according to (83), (84) with $A_0 = 0.01$, $k_0 = 5$, $P = -1.5$, so that for the waves bearing most of the energy the gravity and capillarity forces were of the same order. The time integration was carried out up to $\tau = 1000$ with the time step $\Delta\tau = 0.01$. The dependence of phase velocity (77) and its temporal standard deviation on the wave number is shown in Fig. 13.

As in the runs with pure gravity waves, the lower wave numbers tend to follow the linear dispersion relation (77), though with considerable scattering, while the shorter waves, which are mostly generated by the nonlinear interactions, tend to assume the phase velocities which are characteristic for longer waves and are in this case lower than those given by the linear theory.

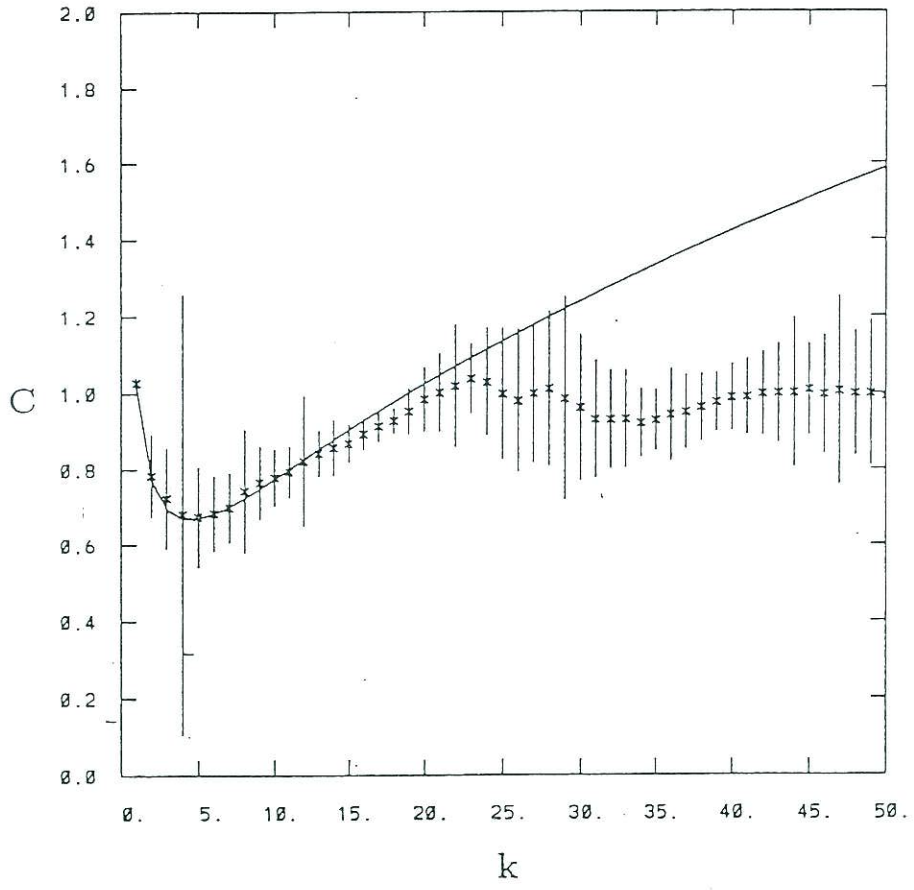

Figure 13: Same as in Fig. 7 but for Exp. 8 (gravity-capillary waves, $\sigma = 0.05$).

The wavenumber spectrum, whose temporal evolution is shown in Fig. 14 in the same way as in Fig. 7 for Exp. 5 and whose mean over the period of integration is represented by Curve 2 in Fig. 15, show a greater nonlinear energy flux to higher wavenumbers than in the case of pure gravity waves. This is manifested in a much less steep slope of the curve, compared to the corresponding results of the previous run (Fig. 12, Curve 6) which was performed with the same initial surface elevation, and in

a relatively fast decrease of energy with time due to dissipation on high wave numbers. The same observation can be made for the frequency spectra (compare Fig. 15, Curve 3 and Fig. 12, Curve 7).

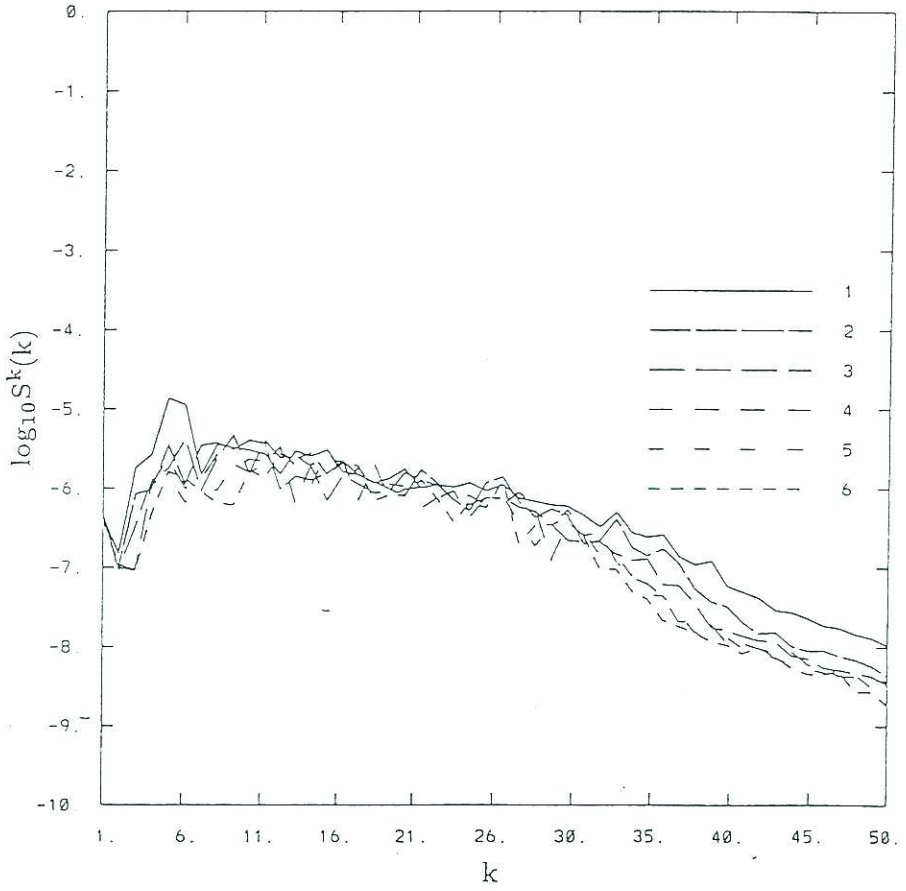

Figure 14: Same as Fig. 6 but for Exp. 8.

In the wavenumber-frequency spectrum (Fig. 15), it is hard to distinguish visually between free and bound waves, since Curve 1 which corresponds to the linear dispersion relation (59) is too close to a straight line, except for the longest waves whose energy is negligibly small. Here, using (59) and regarding that a bound wave propagates with the same phase velocity ω/k as its carrying wave and has a wave number k which is an integer multiple of the latter, we can write the following approximation for the "main branches":

$$\left(\frac{\omega}{n}\right)^2 = \frac{|\,k\,|}{n} + \sigma\left(\frac{|\,k\,|}{n}\right)^3, \tag{87}$$

where $n = 1$ for the free (carrying) waves and $n = 2, 3, \ldots$ for the bound waves. However, the branches appear to merge with each other.

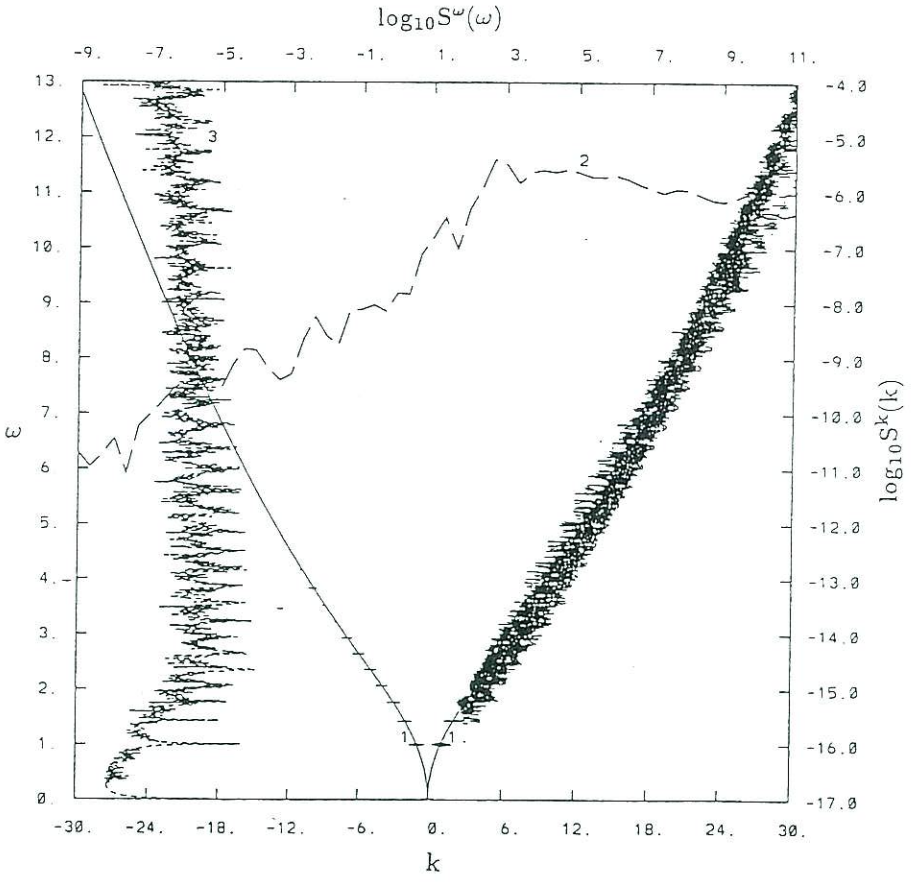

Figure 15: Same spectral characteristics as in Fig. 8 but for Exp. 8. Curve 1 - linear dispersion relation ($n = 1$ in (87)), 2 - $\log_{10} S^k(k)$; 3 - $\log_{10} S(k, \omega)$.

Results of simulation of pure capillary waves (Exp. 9, $\alpha = 0$ in (46)) are shown in Figs. 16 and 17 (the same spectral characteristics as in Figs. 14 and 15 respectively). The initial values of surface elevation were the same as in Exp. 7 and 8; the period of integration was $\tau = 100$, and the time step $\Delta\tau = 0.001$. It is remarkable that the slope of the wavenumber spectrum is much closer to that obtained for pure gravity waves (Exp. 7) than to that of gravity-capillary waves (Exp. 8). The

wavenumber-frequency spectrum agrees well with the linear dispersion relation $\omega = \mid k \mid^{3/2}$ (Curve 1); however, below the curve is what appears to be the set of "main branches" corresponding to bound waves and approximated by

$$\omega^2 = \frac{\mid k \mid^3}{n} \tag{88}$$

(this formula following from (87) with the gravity term omitted and $\sigma = 1$), and there is an additional set of waves above the curve which resembles the "quasi-rectilinear" patterns observed in the pure gravity wave spectra. Fig. 8, 9, 11, 12, 17 may suggest the hypothesis that these patterns correspond to waves which, through nonlinear interactions of modulated shorter waves, are forced to propagate with the group velocities of the latter; further extensive simulations are needed to study this hypothesis.

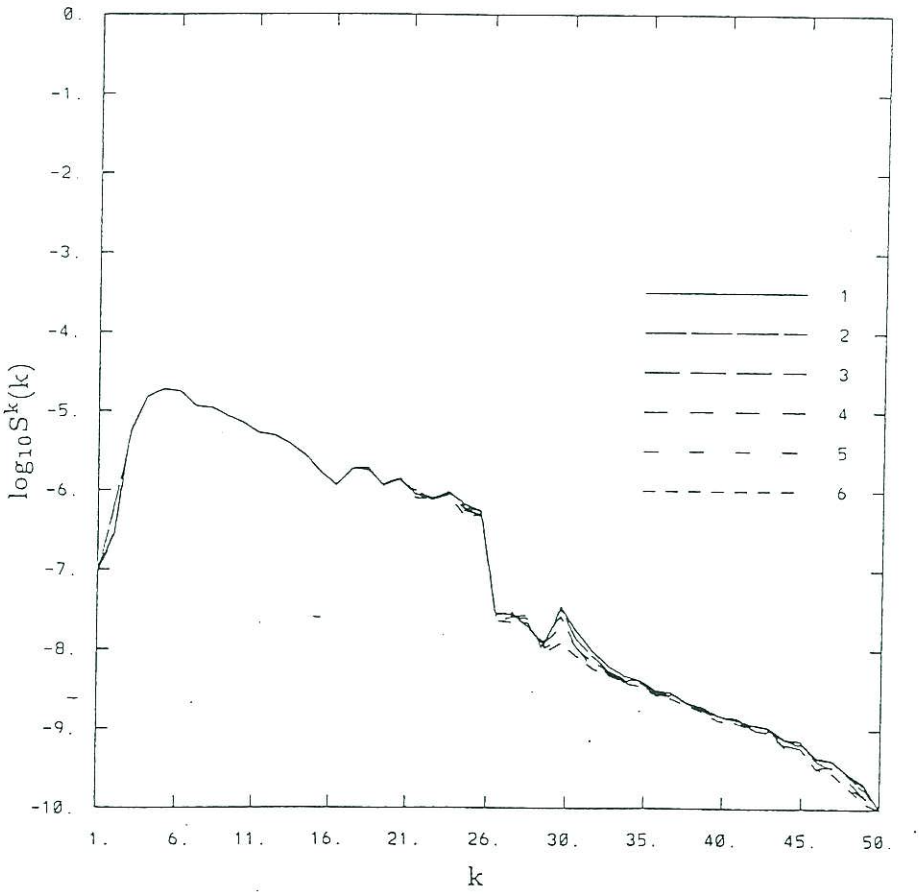

Figure 16: Same as in Fig. 6 but for Exp. 9 (capillary waves), $\delta\tau = 16.7$.

Besides the simulations described above, we ran a number of other experiments with different initial conditions, resolution in the horizontal, and dissipation parameters; some of the runs included various types of external forcing (not discussed here). The wavenumber-frequency spectra observed in all runs had similar features which may be summarized as follows. Most of the energy is concentrated along the curves which were called "main branches" and which consist of free ($n = 1$) and generalized bound ($n = 2, 3, ...$) waves. The general formula for this set of curves is

$$D\left(\frac{\omega}{n}, \frac{k}{n}\right) = 0 \tag{89}$$

and, for not too large k, is approximated by (87) (or (88) for pure capillary waves).

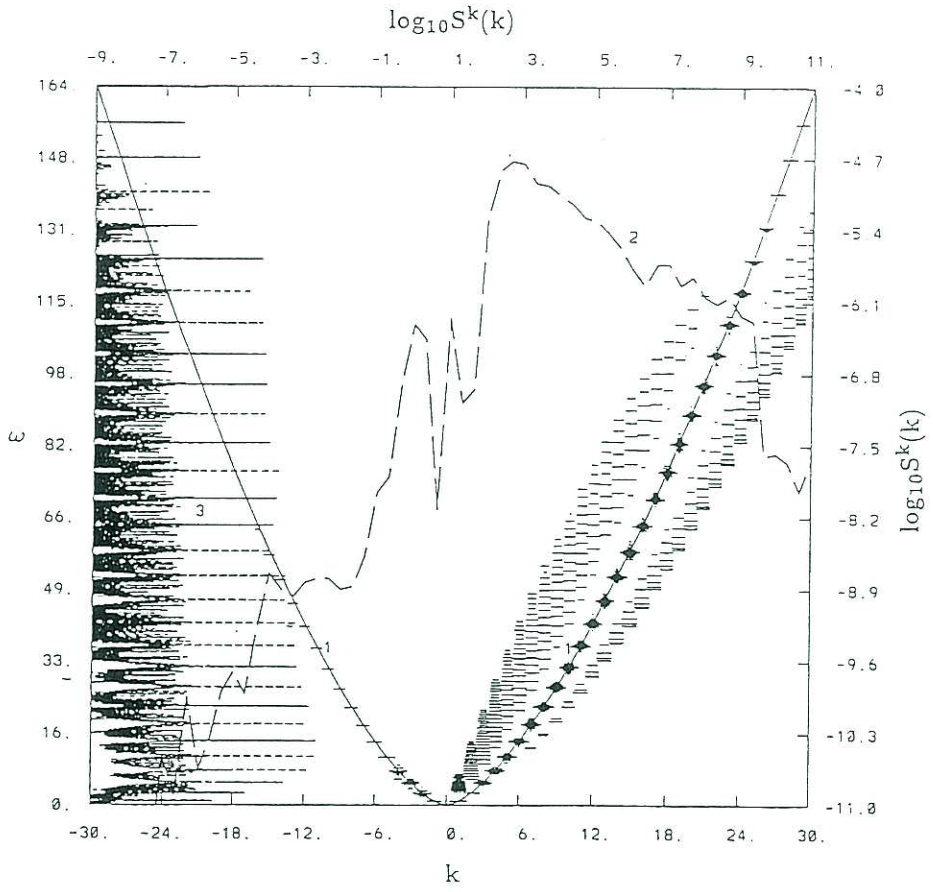

Figure 17: Same as in Fig. 8 but for Exp. 9 (capillary waves), with Curve 1 being the linear dispersion relation (n=1 in (88))

In the dispersion relation (89), nonlinearity is manifested in two ways: first, there is a set of branches instead of one curve corresponding to linear waves; second, the function $D(\omega', k')$ itself differs from its approximation

$$D_l(\omega', k') = \omega'^2 - \mid k' \mid - \sigma \mid k' \mid^3 \tag{90}$$

yielded by the linear theory. The specific form of D depends on the energy distribution over the spectrum and is determined by external forcing and/or the initial conditions. For example, in the very special case of a single progressive wave,

$$D(\omega', k') = \omega' - ck' \tag{91}$$

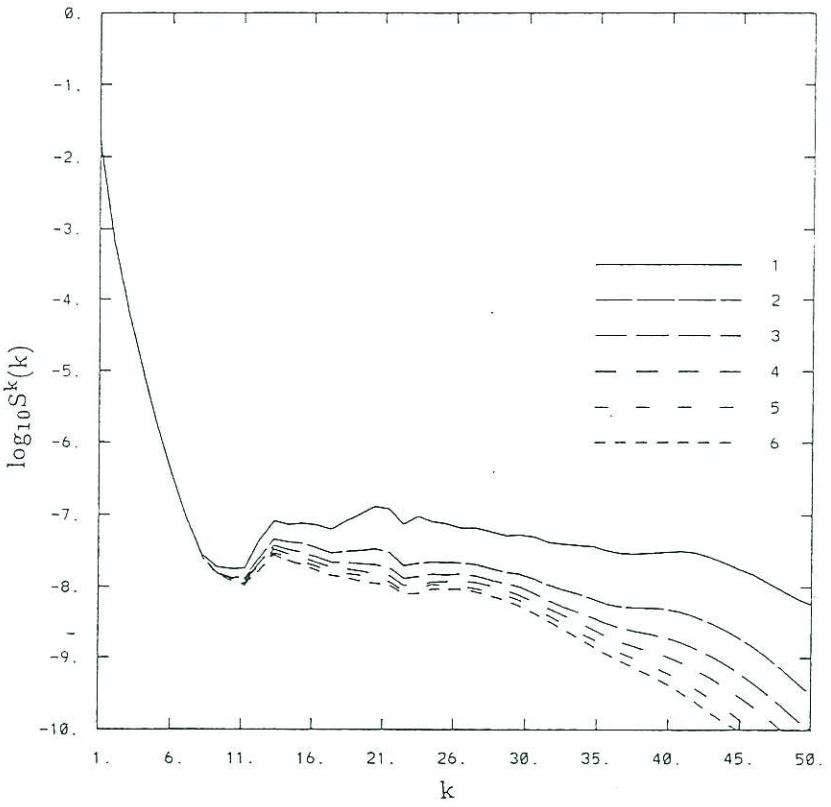

Figure 18: Same as in Fig. 6 but for Exp. 10 (initial conditions: Stokes wave with superimposed short gravity waves).

where c is the phase velocity of the wave; here, each branch consists of one point, and the function D bears no resemblance with (90) except that c can be approximated by the linear phase velocity (59). With increasing k, there is a tendency for the branches to straighten. Along with the "main branches" (89), there are other patterns in the spectra; the corresponding modes bear relatively low energy. These structures need further investigation.

The last model run to be described (Exp. 10) again deals with pure gravity waves and illustrates interaction of a large long wave with small short waves.

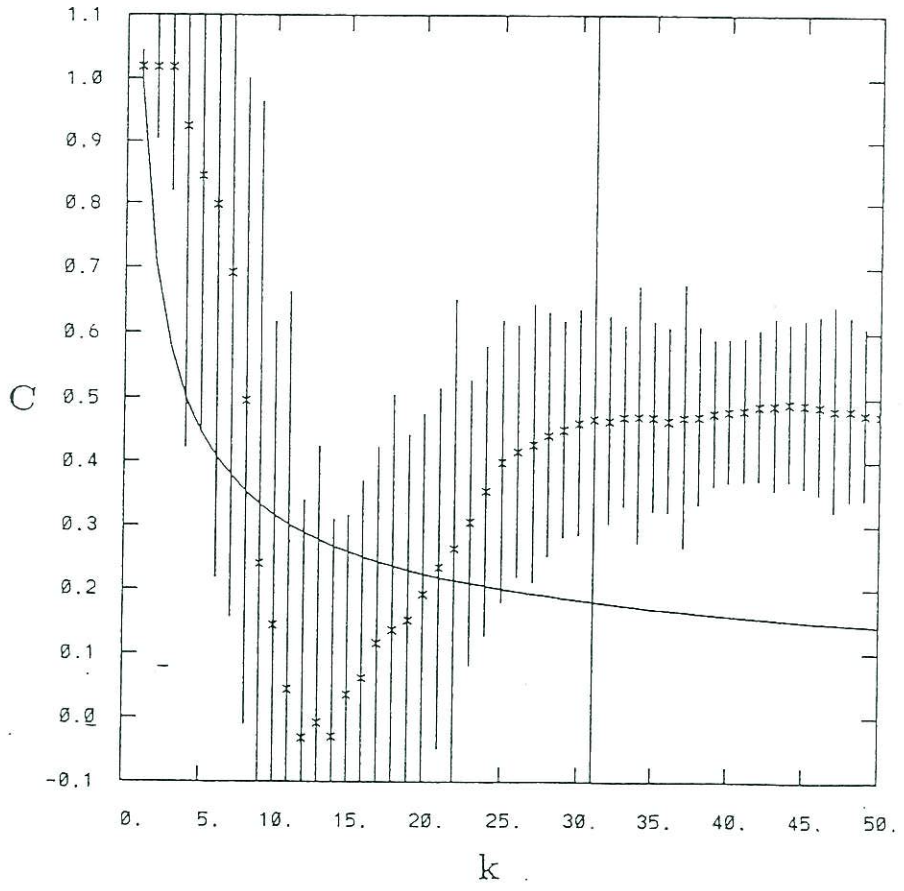

Figure 19: Same as in Fig. 7 but for Exp. 10.

A set of white-noise-like waves with the amplitude of 0.001 in the range $15 \leq k < 40$ was superimposed on a 2π - periodic Stokes wave with the

amplitude $A = 0.3$. The integration was performed up to $\tau = 1000$ with $\Delta\tau = 0.01$.

Time evolution of the wavenumber spectrum is given in Fig. 18 which shows that the energy of the main Fourier components of Stokes wave remained virtually unchanged while the energy of the short waves decreased considerably during the integration. The dependence of phase velocity (77) on wave number differs substantially from the corresponding results of the previously described runs: it bears little resemblance with the linear-theory dependence (59) (the curve in Fig. 19).

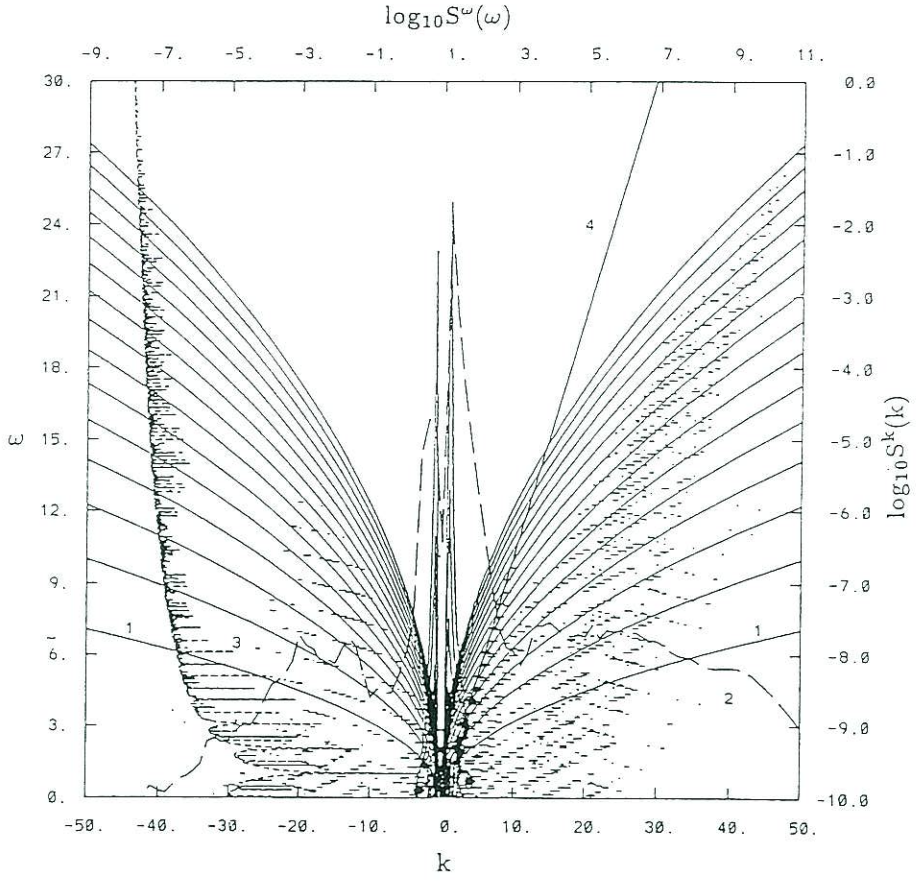

Figure 20: Same spectral characteristicsas in Fig 8 but for Exp. 10. Curve 1 - linear dispersion relation $\omega^2 = k$, 2 - $\log_{10} S^k(k)$; 3 - $\log_{10} S^\omega(\omega)$, 4 - components of the Stokes wave ($\omega = ck$).

Correspondingly, in the wavenumber-frequency spectra (Fig. 20) the

"main branches" (89) appear to be represented only by the Fourier components of the Stokes wave and so are described by (91), while the superimposed waves belong to additional regular patterns which are completely different from those observed in Exp. 6 (Fig. 11) where "pure" white noise was used as the the inintial conditions. The difference suggests that the behavior of the superimposed waves is strongly controlled by interactions with the Stokes wave. The same conclusion can be drawn from the fact that the distribution of the energy density of the short waves over the phase of the Stokes wave (Fig. 21) is far from uniform or chaotic, and show clear maxima at the points of maximum slope of the Stokes wave.

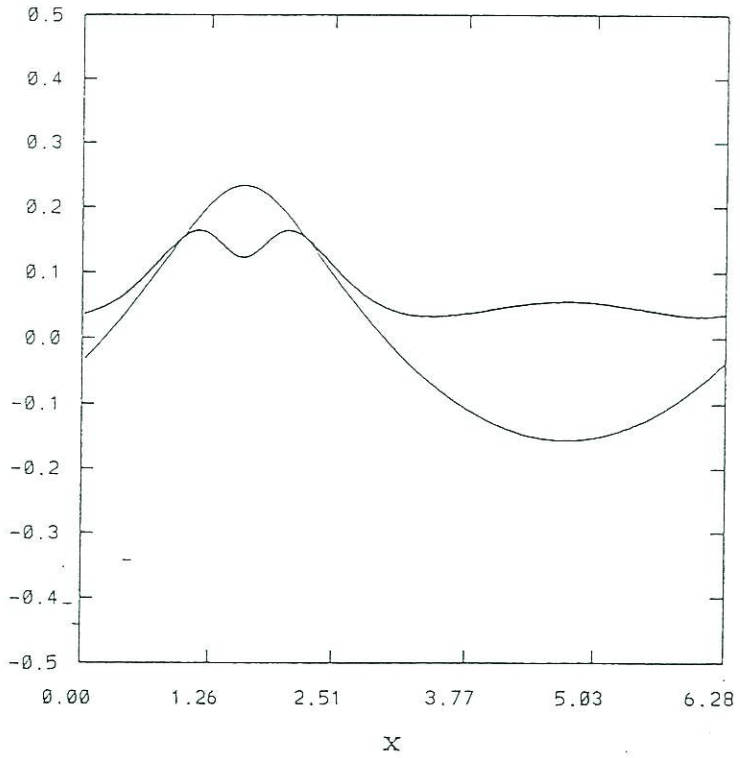

Figure 21: Distribution of the time-averaged potential energy of perturbations (multiplied by 100, thick curve) over the phase of the running Stokes-like wave (thin curve, obtained by time averaging of the surface profile) (Exp. 10). The averaging is performed in a coordinate system moving with the component $k = 1$.

Conclusions

The behavior of nonlinear waves is difficult to investigate analytically. Even for the stationary equations, exact solutions are known only in the isolated case of pure capillary (Crapper's) waves. In the case of stationary pure gravity (Stokes) waves, construction of analytical expansions for consecutive Fourier coefficients provides only an approximation for truncated Fourier series and is thus, actually, a numerical procedure in which the amount of calculations increases sharply with increasing truncation number. As for general nonstationary wave fields, their analytical investigation is clearly impossible without drastic simplifications which may lead to unpredictable consequences. In the development of numerical algorithms for 1-D potential waves, considerable progress has been made during the last 15 years, but the applicability of these techniques for simulation of multi-mode wave fields over a long time period has not been proven. One possible approach to circumvent these problems is to develop a highly accurate numerical scheme for the principal equations of potential waves. With such a scheme, direct hydrodynamical modeling of wave phenomena may be expected to provide improvements in many theoretical and applied aspects of wave studies.

The main difficulty in constructing numerical methods for nonstationary potential vaves is how to deal with the vertical dimension which, in order to simplify the problem, must be eliminated from the model prognostic equations which are to be solved by numerical time integration. The nonstationary surface-following conformal mapping used in our scheme is, indeed, a most effective way to resolve this problem and make the model capable of long-term multi-mode simulations.

The results obtained in this work may be divided into three groups.

1. The method of conformal mapping developed by Stokes (1848) for stationary potential waves was extended to the nonstationary case, where the conformal transformation becomes time dependent, and the surface-following coordinates are no longer the velocity potential and the stream function. The method proved effective because the original system consisting of a Laplace equation and two nonlinear boundary conditions on a curvilinear surface are reduced, without any simplification, to a system

of two one-dimensional nonstationary equations. As in the Cartesian coordinates, the dependent variables are the elevation and the velocity potential of the surface, but their dependence on the Cartesian horizontal coordinate x is represented parametrically via the new horizontal coordinate ξ. The transformed system may be solved by numerical integration, which is done efficiently by calculating nonlinearities via Fourier transform method. The system may also be used for analytical investigations based on various methods developed for the original system, with the important advantage that the problem of extapolating the velocity potential in the vertical does not exist.

2. A numerical method for solution of the stationary equations for gravity and gravity-capillary waves has been developed. The method allows us to obtain the solutions with computer accuracy and is based on representation of the differential equation for the surface height, written in the new coordinates (which in this case are proportional to the velocity potential and the stream function) via operators of integration and (generalized) Hilbert transformation calculated in Fourier space. Again, the use of Fourier transform method to calculate nonlinearities allows a highly efficient implementation of the method. It should be noted that we had to develop two separate algorithms for pure gravity and gravity-capillary waves, and that in the latter case our algorithm fails to converge when the nondimensional capillarity coefficient becomes small. This problem will require further investigations. It was shown that, with decreasing values of capillarity coefficient, the phase velocities of gravity-capillary waves decrease rather than approach the values of the Stokes phase velocity. Thus, the Stokes waves do not appear to be an asymptotic form of the gravity-capillary waves as the capillarity goes to zero. This, together with non-convergence of the algorithm (and its various modifications) for small capillarities, may be an indication that stationary gravity-capillary waves which are only slightly affected by capillary forces are unstable or simply do not exist.

While properties of stationary solutions imply many intriguing problems, we used these results mainly as a tool to validate the nonstationary model. The validation was performed by using solutions obtained in section 3 as initial conditions for the nonstationary problem. Since the coordinate system of the latter was bound to the mean flow rather than to the wave profile, the model simulates running Stokes and gravity-capillary

waves. It should be emphasized that the validation was far from trivial, as the nonstationary model is based on equations much more complicated than the stationary ones and on a numerical procedure of its own, which "does not know" that the simulated waves are supposed to retain their shape. Nevertheless, they did retain it surprisingly well even for large amplitudes. This suggests that (1) Stokes and gravity-capillary waves are stable with respect to truncation errors of the nonstationary model, and (2) these errors are small enough.

3. We used the nonstationary model for case studies of evolution of nonlinear wave fields. The cases described in section 6 were chosen somewhat arbitrarily, as our aim was to provide a possibly broader variety of applications of the technique developed. The effects of bound waves were most clearly seen in the simulation designed to approximate the laboratory experiment by Yuen and Lake (1982). A most surpising feature of multi-mode wave fields was a clear separation of the wavenumber-frequency spectra into regular curvilinear branches, with most of the energy concentrated along what we called "main branches". This set of branches satisfies a dispersion relation whose form is given by (89) where the number n of the branch is 1 for the branch consisting of free waves and is greater than 1 for branches consisting of generalized bound waves. In this structure, nonlinear effects were manifested both in the existence of multiple branches and in deviation of the "parent" curve ($n = 1$) from the linear dispersion relation for relatively large wave numbers. In most cases the deviation clearly appeared to be such that the curve approaches a straight line and so the group velocity tends to a constant; however, this effect needs further analysis. The nonlinear interactions also produced other regular branches. The energy of the modes belonging to these additional branches was usually very small, sometimes with the remarkable exception of a peculiar pattern (or group of patterns) which, at least for wave numbers that are not too small, could be roughly approximated by a straight line passing through the origin. The nonlinear behavior was perhaps most strongly manifested in the case of a long Stokes wave with superimposed small short waves, where the free wave branch is poorly represented, and propagation of short waves is largely controlled by interactions with the Stokes wave. On the other hand, the nonlinear energy flux to higher wavenumbers was remarkably larger in the case of gravity-capillary waves than in all other runs, which included pure gravity and pure capillary waves simulations with the same initial

surface hight. This case also needs further investigation, as the structure of the wavenumber-frequency specrtum was partially obscured by apparent merging of the branches.

The technique developed here may be used to study a variety of problems of the nonlinear wave dynamics:

- spectral properties of nonlinear wave fields in a wide range of wave numbers, depths and capillarity coefficients;

- coupling between short and long waves;

- validation of kinematic wave models by use of the developed hydrodynamical model as a generator of moving wave surfaces;

- wind-wave interaction, which can be studied by coupling of the described model with a wave boundary layer model (e. g. Chalikov, 1986).

Acknowledgements

The authors wish to thank Prof. V. Zakharov for helpful discussions and the advice to use the Hilbert transform to resolve the model equations with respect to the time derivatives; Dr. D. B. Rao, Dr. W. Perrie, and Dr. L. Breaker for reading the manuscript and making many valuable comments.

References

Chalikov D.V. 1976 A mathematical model of wind-induced waves. *Dokl. Acad. Nauk SSSR*, **229**, 1083-1086.

Chalikov D.V. 1978 Numerical simulation of wind-wave interaction. *J. Fluid. Mech.* **87**, 561-582.

Chalikov D.V., 1986 Numerical simulation of the boundary layer above waves. *Bound. Layer Met.*, 1986, No.34. 63-98.

Chalikov D.V., & Liberman Yu. M. 1991 Integration of primitive equations for potential waves. *Izv.Sov.Atm.Ocean Phys.* **27**,42-47.

Chalikov, D., 1995: The Parameterization of the Wave Boundary Layer. *J. Phys. Oceanogr.*, **25**, 1335-1349.

Craig, W. & Sulem, C. 1993 Numerical Simulation of Gavity Waves. *J. Comp. Phys.* **108**, 73-83.

Crapper, G. D., 1957 An exact solution for progressive capillary waves of arbitrary amplitude. *J. Fluid Mech.*, **96** ,417-445.

Crapper, G. D. 1984 Introduction to water waves. John Willey & Sons. 224 pp.

Dold J.W. 1992 A Efficient Surface-Integral Algorithm Applied to Unsteady Gravity Waves. *J. Comp. Phys.*, **103** 90-115.

Donelan M. A. & Hui W. H. 1990 Mechanics of ocean surface waves. *In: Surface Waves and Fluxes* edited by G. L. Geernaert and W. J. Plant. Kluwer Acad. Publ. v. 1, 209-246.

Drennan, W. M., Hui, W. N. Tenti G. 1992 Accurate calculatioms of Stokes water waves of large amplitude. *Z. angew Math. Phys.*, bf 43, 367-380.

Eliassen, E.,B., B. Machenhauer, B. & Rasmussen, E. 1970 On a numerical method for integration of the hydro-dynamical equations with a spectral representation of the horiszontal fields. Report No.2, Institute for Teoretisk. Meteorologi, Københavens Universitet, Copenhagen, Denmark.

Hasselmann, K., T.P. Barnett, E. Bouws, H. Carlson, D.E. Cartwright, K. Enke, J.A. Ewing, H. Gienapp, D.E. Hasselmann, P. Kruseman, A. Meerburg, P. Müller, D.J. Olbers, K. Richter, W. Sell and H. Walden, 1973: Measurements of wind-wave growth and swell decay during the Joint North Sea Wave Project. *Ergánzungsheft zur Deutschen Hydrographischen Zeitschrift*, Reihe A (8) Nr. 12, 95 pp.

Hasselmann, K. 1962 On the nonl,inear energy transfer in a gravity-wave spectrum, part 1: General theory. *J. Fluid Mech.*, bf 12, 481-500.

Kahma, K.K. and C.J. Calkoen, 1992: Reconciling discrepancies in the observed growth rates of wind waves. *J. Phys. Oceanogr.*, **22**, 1389-1405.

Kuznetsov, E. A., Spector, M. D. & Zakharov, V. E. 1994 Formation of singularities on the free surface of an ideal fluid. *Physical review*, bf 49, No. 2, 1283-1290.

Lake, B. M. & H. C. Yuen 1978 A new model for nonlinear wind waves. Part. Physical model and experimental evidencce *J. Fluid Mech.*, **88**, 33-62.

Longuet-Higgins M. S. Integral properties of periodic gravity waves of finite amplitude. *Proc. R. Soc. Lond.* A **342**, 157-174.

Longuet-Higgins M. S. & Cokelet E. D. 1976 The deformation of steep surface waves on water. I. A numerical method of computation *Proc. R. Soc. Lond. Ser. A* **350**, 1-26.

Orszag, S.A. 1970 Transform method for calculation of vector coupled sums. Application to the spectral form of vorticity equation, *J. Atmos. Sci.* **27**, 890-895.

Prosperetti, A. & Jacobs J. W. 1983 A Numerical Method for Potential Flow with a Free Surface. *J. Comp. Phys.*, **51**,365-386.

Stokes, G.G. 1847 On the theory of oscillatory waves. *Trans. Cambridge Philos. Soc.*. **8**, 441-445. *Math. Phys. Pap.*, **1** 197-229.

Stokes, G.G. 1880 Supplement to a paper on the theory of oscillatory waves. *Math. Phys. Pap.*, **1** 314-326.

Watson, K. M. & West B.J. 1975 A transport-equation description of nonlinear ocean surface wave interactions. *J. Fluid Mech.*, **70**, 815-826.

West B. J. Brueckner K. A. & Janda R. S 1987 A New Numerical Method for Surface Hydrodynamics. *J. Geophys. Res.* **92**, No. C11 11,803-11,824.

Yuen, H. C. & B. M. Lake, 1982 Nonlinear nDynamics of Deep-Water Gravity Waves.*Adv. in Appl. Mech.*,**22**, 67-229.

Zakharov, V. E. 1968 Stability of periodic waves of finite am[plitude on the surface of a deep fluid.*J. Appl. Mech. Tech. Phys. (Engl. Transl.)* **2**, 190-194.

No. 21. Breaker, L. C., 1989: El Nino and Related Variability PACLIM Monograph of Climate Variability of the Ea Monograph 55, AGU, 133-140.

No. 22. Yu, T. W., D. C. Esteva, and R. L. Teboulle, 1991: A Data at the National Meteorological Center. Technical

No. 23. Burroughs, L. D., 1989: Open Ocean Fog and Visibili Note No. 348, 18pp.

No. 24. Gerald, V. M., 1987: Synoptic Surface Marine Data M

No. 25. Breaker, L. C., 1989: Estimating and Removing Sens Geophysical Reseach, 95, 9701-9711.

No. 26. Chen, H. S., 1990: Infinite Elements for Water Wave Methods in Fluids, 11, 555-569.

No. 27. Gemmill, W. H., T. W. Yu, and D. M. Feit, 1988: A S Winds. Journal of Weather and Forecasting, 3, 153-16

No. 28. Rao. D. B., 1989: A Review of the Program of the Oce

No. 29. Chen, H. S., 1989: Infinite Elements for Combined Di International Conference on Finite Element Methods F

No. 30. Chao, Y. Y., 1989: An Operational Spectral Wave For International Workshop on Wave Forecasting and Hin

No. 31. Esteva, D. C., 1989: Improving Global Wave Forecast International Workshop on Wave Hindcasting and For

No. 32. Richardson, W. S., J. M. Nault, and D. M. Feit, 1989: C Coastal Ocean Management Coastal Zone 89, 4075-408

No. 33. Chao, Y. Y., and T. L. Bertucci, 1989: A Columbia Riv Products Center. Techical Note/NMC Office Note 361.

No. 34. Burroughs, L. D., 1989: Forecasting Open Ocean Fog a Statisitcs, Monterey, Ca., 5pp.

No. 35. Rao, D. B., 1990: Local and Regional Scale Wave Mod WMO, Marine Meteorological of Related Oceanograph

No. 36. Burroughs, L.D., 1991: Forecast Guidance for Santa An

No. 37. Burroughs, L. D., 1989: Ocean Products Center Product 359. 29pp.

No. 38. Feit, D. M., 1989: Compendium of Marine Meteorologi (revision 1). NOAA Technical Memo NWS/NMC 68.

No. 39. Esteva, D. C., and Y. Y. Chao, 1991: The NOAA Ocea Spectra, Johns Hopkins University Press, 163-166.

No. 40. Sanchez, B. V., D. B. Rao, and S. D. Steenrod, 1987: T Solution. NASA Technical Memorandum 87812, 18pp.

No. 41. Crosby, D. S., L. C. Breaker, and W. H. Gemmill, 1990: A Defintion for Vector Correlation and its Application to Marine Surface Winds. Technical Note/NMC Office Note No. 365, 52pp.

No. 42. Feit, D. M., and W. S. Richardson, 1990: Expert System for Quality Control and Marine Forecasting Guidance. Preprint, 3rd Workshop Operational and Metoerological. CMOS, 6pp.

No. 43. Gerald, V. M., 1990: OPC Unified Marine Database Verification System. Technical Note/NMC Office Note No. 368, 14pp.

No. 44. Wohl, G. M., 1990: Sea Ice Edge Forecast Verification System. National Weather Association Digest, (submitted)

No. 45. Feit, D. M., and J. A. Alpert, 1990: An Operational Marine Fog Prediction Model. NMC Office Note No. 371, 18pp.

No. 46. Yu, T. W., and R. L. Teboulle, 1991: Recent Assimilation and Forecast Experiments at the National Meteorological Center Using SEASAT-A Scatterometer Winds. Technical Note/NMC Office Note No. 383, 45pp.

No. 47. Chao, Y. Y., 1990: On the Specification of Wind Speed Near the Sea Surface. Marine Forecaster Training Manual.

No. 48. Breaker, L. C., L. D. Burroughs, T. B. Stanley, and W. B. Campbell, 1992: Estimating Surface Currents in the Slope Water Region Between 37 and 41°N Using Satellite Feature Tracking. Technical Note, 47pp.

No. 49. Chao, Y. Y., 1990: The Gulf of Mexico Spectral Wave Forecast Model and Products. Technical Procedures Bulletin No. 381, 3pp.

No. 50. Chen, H. S., 1990: Wave Calculation Using WAM Model and NMC Wind. Preprint, 8th ASCE Engineering Mechanical Conference, 1, 368-372.

No. 51. Chao, Y. Y., 1990: On the Transformation of Wave Spectra by Current and Bathymetry. Preprint, 8th ASCE Engineering Mechnical Conference, 1, 333-337.

No. 52. WAS NOT PUBLISHED

No. 53. Rao, D. B., 1991: Dynamical and Statistical Prediction of Marine Guidance Products. Proceedings, IEEE Conference Oceans 91, 3, 1177-1180.

No. 54. Gemmill, W. H., 1991: High-Resolution Regional Ocean Surface Wind Fields. Proceedings, AMS 9th Conference on Numerical Weather Prediction, Denver, CO, Oct. 14-18, 1991, 190-191.

No. 55. Yu, T. W., and D. Deaven, 1991: Use of SSM/I Wind Speed Data in NMC's GDAS. Proceedings, AMS 9th Conference on Numerical Weather Prediction, Denver, CO, Oct. 14-18, 1991, 416-417.

No. 56. Burroughs, L. D., and J. A. Alpert, 1993: Numerical Fog and Visiability Guidance in Coastal Regions. Technical Procedures Bulletin. No. 398, 6pp.

No. 57. Chen, H. S., 1992: Taylor-Gelerkin Method for Wind Wave Propagation. ASCE 9th Conf. Eng. Mech. (in press)

No. 58. Breaker, L. C., and W. H. Gemmill, and D. S. Crosby, 1992: A Technique for Vector Correlation and its Application to Marine Surface Winds. AMS 12th Conference on Probability and Statistics in the Atmospheric Sciences, Toronto, Ontario, Canada, June 22-26, 1992.

No. 59. Yan, X.-H., and L. C. Breaker, 1993: Surface Circulation Estimation Using Image Processing and Computer Vision Methods Applied to Sequential Satellite Imagery. Photogrammetric Engineering and Remote Sensing, 59, 407-413.

No. 60. Wohl, G., 1992: Operational Demonstration of ERS-1 SAR Imagery at the Joint Ice Center. Proceeding of the MTS 92 - Global Ocean Partnership, Washington, DC, Oct. 19-21, 1992.

No. 61. Waters, M. P., Caruso, W. H. Gemmill, W. S. Richardson, and W. G. Pichel, 1992: An Interactive Information and Processing System for the Real-Time Quality Control of Marine Meteorological Oceanographic Data. Pre-print 9th International Conference on Interactive Information and Processing System for Meteorology, Oceanography and Hydrology, Anaheim, CA, Jan. 17-22, 1993.

No. 62. Breaker, L. C., and V. Krasnopolsky, 1994: The Problem of AVHRR Image Navigation Revisited. Int. Journal of Remote Sensing, 15, 979-1008.

No. 63. Crosby, D. S., L. C. Breaker, and W. H. Gemmill, 1993: A Proposed Definition for Vector Correlation in Geophysics: Theory and Application. Journal of Atmospheric and Ocean Technology, 10, 355-367.

No. 64. Grumbine, R., 1993: The Thermodynamic Predictability of Sea Ice. Journal of Glaciology, 40, 277-282, 1994.

No. 65. Chen, H. S., 1993: Global Wave Prediction Using the WAM Model and NMC Winds. 1993 International Conference on Hydro Science and Engineering, Washington, DC, June 7 - 11, 1993. (submitted)

No. 66. WAS NOT PUBLISHED

No. 67. Breaker, L. C., and A. Bratkovich, 1993: Coastal-Ocean Processes and their Influence on the Oil Spilled off San Francisco by the M/V Puerto Rican. Marine Environmental Research, 36, 153-184.

No. 68. Breaker, L. C., L. D. Burroughs, J. F. Culp, N. L. Gunasso, R. Teboulle, and C. R. Wong, 1993: Surface and Near-Surface Marine Observations During Hurricane Andrew. Technical Note/NMC Office Note #398, 41pp.

No. 69. Burroughs, L. D., and R. Nichols, 1993: The National Marine Verification Program - Concepts and Data Management, Technical Note/NMC Office Note #393, 21pp.

No. 70. Gemmill, W. H., and R. Teboulle, 1993: The Operational Use of SSM/I Wind Speed Data over Oceans. Pre-print 13th Conference on Weather Analyses and Forecasting, AMS Vienna, VA., August 2-6, 1993, 237-238.

No. 71. Yu, T.-W., J. C. Derber, and R. N. Hoffman, 1993: Use of ERS-1 Scatterometer Backscattered Measurements in Atmospheric Analyses. Pre-print 13th Conference on Weather Analyses and Forecasting, AMS, Vienna, VA., August 2-6, 1993, 294-297.

No. 72. Chalikov, D. and Y. Liberman, 1993: Director Modeling of Nonlinear Waves Dynamics. J. Physical, (To be submitted).

No. 73. Woiceshyn, P., T. W. Yu, W. H. Gemmill, 1993: Use of ERS-1 Scatterometer Data to Derive Ocean Surface Winds at NMC. Pre-print 13th Conference on Weather Analyses and Forecasting, AMS, Vienna, VA, August 2-6, 1993, 239-240.

No. 74. Grumbine, R. W., 1993: Sea Ice Prediction Physics. Technical Note/NMC Office Note #396, 44pp.

No. 75. Chalikov, D., 1993: The Parameterization of the Wave Boundary Layer. Journal of Physical Oceanography, Vol. 25, No. 6, Par 1, 1333-1349.

No. 76. Tolman, H. L., 1993: Modeling Bottom Friction in Wind-Wave Models. Ocean Wave Measurement and Analysis, O.T. Magoon and J.M. Hemsley Eds., ASCE, 769-783.

No. 77. Breaker, L., and W. Broenkow, 1994: The Circulation of Monterey Bay and Related Processes. Oceanography and Marine Biology: An Annual Review, 32, 1-64.

No. 78. Chalikov, D., D. Esteva, M. Iredell and P. Long, 1993: Dynamic Coupling between the NMC Global Atmosphere and Spectral Wave Models. Technical Note/NMC Office Note #395, 62pp.

No. 79. Burroughs, L. D., 1993: National Marine Verification Program - Verification Statistics - Verification Statistics, Technical Note/NMC Office Note #400, 49 pp.

No. 80. Shashy, A. R., H. G. McRandal, J. Kinnard, and W. S. Richardson, 19 93: Marine Forecast Guidance from an Interactive Processing System. 74th AMS Annual Meeting, January 23 - 28, 1994.

No. 81. Chao, Y. Y., 1993: The Time Dependent Ray Method for Calculatio n of Wave Transformation on Water of Varying Depth and Current. Wave 93 ASCE.

No. 82. Tolman, H. L., 1994: Wind-Waves and Moveable-Bed Bottom Fricti on. Journal of Physical Oceanography, 24, 994-1009.

No. 83. Grumbine, R. W., 1993: Notes and Correspondence A Sea Ice Albed o Experiment with the NMC Meduim Range Forecast Model. Weather and Forecasting, (submitted).

No. 84. Chao, Y. Y., 1993: The Gulf of Alaska Regional Wave Model. Tech nical Procedure Bulletin, No. 427, 10 pp.

No. 85. Chao, Y. Y., 1993: Implementation and Evaluation of the Gulf of Alas ka Regional Wave Model. Technical Note, 35 pp.

No. 86. WAS NOT PUBLISHED.

No. 87. Burroughs, L., 1994: Portfolio of Operational and Development Marin e Meteorological and Oceanographic Products. Technical Note/NCEP Office Note No. 412, 52 pp. [PB96-158548]

No. 88. Tolman, H. L., and D. Chalikov, 1994: Development of a third-genera tion ocena wave model at NOAA-NMC. Proc. Waves Physical and Numberial Modelling, M. Isaacson and M.C. Quic k Eds., Vancover, 724-733.

No. 89. Peters, C., W. H. Gemmill, V. M. Gerald, and P. Woiceshyn, 1994: Ev aluation of Empirical Transfer Functions for ERS-1 Scatterometer Data at NMC. 7th Conference on Satellite Meteo rology and Oceanography, June 6-10, 1994, Monterey, CA., pg. 550-552.

No. 90. Breaker, L. C., and C. R. N. Rao, 1996: The Effects of Aerosols from the Mt. Pinatubo and Mt. Hudson Volcanio Eruption on Satellite-Derived Sea Surface Temperatures. Journal of Ge ophysical Research. (To be submitted).

No. 91. Yu, T-W., P. Woiceshyn, W. Gemmill, and C. Peters, 1994: Analysis & Forecast Experiments at NMC Using ERS-1 Scatterometer Wind Measurements. 7th Conference on Satellite Mete orology and Oceanography, June 6-10, 1994, Monterey, CA., pg. 600-601.

No. 92. Chen, H. S., 1994: Ocean Surface Waves. Technical Procedures Bulle tin, No. 426, 17 pp.

No. 93. Breaker, L. C., V. Krasnopolsky, D. B. Rao, and X.-H. Yan, 1994: The Feasibility of Estimating Ocean Surface Currents on an Operational Basis using Satellite Feature Tracking Meth ods. Bulletin of the American Meteorolgical Society, 75, 2085-2095.

No. 94. Krasnopolsky V., L. C. Breaker, and W. H. Gemmill, 1994: Developm ent of Single "All-Weather" Neural Network Algorithms for Estimating Ocean Surface Winds from the Special Sens or Microwave Imager. Technical Note.

No. 95. Breaker, L. C., D. S. Crosby and W. H. Gemmill, 1994: The applicatio n of a New Definition for Vector Correlation to Problems in Oceanography and Meteorology. Journal of Applied Mete orology, 33, 1354-1365.

No. 96. Peters, C. A., V. M. Gerald, P. M. Woiceshyn, and W. H. Gemmill, 199 4: Operational Processing of ERS-1 Scatterometer winds: A Documentation. Technical Note.

No. 97. Gemmill, W. H., P. M. Woiceshyn, C. A. Peters, and V. M. Gerald, 199 4: A Preliminary Evaluation Scatterometer Wind Transfer Functions for ERS-1 Data. Technical Note.

No. 98. Chen, H. S., 1994: Evaluation of a Global Ocean Wave Model at NMC . International Conference on Hydro-Science and Engineering. Beijing, China, March 22 - 26, 1995.

No. 99. Aikman, F. and D. B. Rao, 1994: NOAA Perspective on a Coastal Forecast System.

No. 100. Rao, D. B. and C. Peters, 1994: Two-Dimensional Co-Oscillations in a Rectangular Bay: Possible Application to Water-Level Problems. Marine Geodesy, 18, 317-332.

No. 101. Breaker, L. C., L. D. Burroughs, Y. Y. Chao, J. F. Culp, N. L. Gunasso, R. Teboulle, and C. R. Wong, 1994: Surface and Near-Surface Marine Observations During Hurricane Andrew. Weather and Forecasting, 9, 542-556.

No. 102. Tolman, H. L., 1995: Subgrid Modeling of Moveable-bed Bottom Friction in Wind Wave Models. Coastal Engineering, (in press).

No. 103. Breaker, L. C., D. B. Gilhousen, H. L. Tolman and L. D. Burroughs, 1995: Initial Results from Long-Term Measurements of Atmospheric Humidity and Related Parameters the Marine Boundary Layer at Two Locations in the Gulf of Mexico. (To be submitted to Global Atmosphere and Ocean Systems).

No. 104. Burroughs, L. D., and J. P. Dallavalle, 1995: Great Lakes Wind and Wave Guidance. Technical Procedures Bulletin No., (In preparation).

No. 105. Burroughs, L. D., and J. P. Dallavalle, 1995: Great Lakes Storm Surge Guidance. Technical Procedures Bulletin No., (In preparation).

No. 106. Shaffer, W. A., J. P. Dallavalle, and L. D. Burroughs, 1995: East Coast Extratropical Storm Surge and Beach Erosion Guidance. Technical Procedures Bulletin No., (In preparation)

No. 107. WAS NOT PUBLISHED.

No. 108. WAS NOT PUBLISHED.

No. 109. WAS NOT PUBLISHED.

No. 110. Gemmill, W. H, and C. A. Peters, 1995: The Use of Satellite Dervired Wind Data in High-Resolution Regional Ocean Surface Wind Fields. Conference on Coastal Oceanic and Atmospheric Prediction, Jan 28 - Feb 2, 1996, Atlanta, GA (accepted at preprint press).

OPC CHANGES TO OMB

No. 111. Krasnopolsky, V. M, W. H. Gemmill, and L. C. Breaker, 1995: Improved SSM/I Wind Speed Retrievals at Higher Wind Speeds. Journal of Geophysical Research, (in press).

No. 112. Chalikov, D., L. D. Breaker, and L. Lobocki, 1995: A Simple Model of Mixing in the Upper Ocean. Journal of Physical Ocean, (in press).

No. 113. Tolman, H. L., 1995: On the Selection of Propagation Schemes for a Spectral Wind-Wave Model. NCEP Office Note No. 411.

No. 114. Grumbine, R. W., 1995: Virtual Floe Ice Drift Forecast Model Intercomparison. NCEP Office Note. (To be submitted).

No. 115. Grumbine, R. W., 1995: Sea Ice Forecast Model Intercomparison: Selecting a Base Model for NCEP Sea Ice Modelling. Technical Note.

No. 116. Yu, T. W. and J. C. Derber, 1995: Assimilation Experiments with ERS-1 Winds: Part I - Use of Backscatter Measurements in the NMC Spectral Statistical Analysis System. Technical Note.

No. 117. Yu, T. W., 1995: Assimilation Experiments with ERS1 Winds: Part II - Use of Vector Winds in NCEP Spectral Statistical Analysis System. Technical Note.

No. 118. Grumbine, R. W., 1995: Sea Ice Drift Guidance. Technical Procedures Bulletin. (submitted)

No. 119. Tolman, H. L., 1996: Statistical Model Validation Techniques Applied to Marine Wind Speed Analysis. Technical Note.

No. 120. Grumbine, R. W., 1996: Automated Passive Microwave Sea Ice Concentration Analysis at NCEP. Technical Note.

No. 121. Grumbine, R. W., 1996: Sea Ice Prediction Environment: Documentation. Technical Note.

No. 122. Tolman, H. L and D. Chalikov, 1996: On the Source Terms in a Third-Generation Wind Wave Model. Journal of Physical Oceanography. (To be submitted).

No. 123. Gemmill, W. H., V. Krasnopolsky, L. C. Breaker, and C. Peters, 1996: Developments to Improve Satellite Derived Ocean Surface Winds for use in Marine Analyses. Pre-print Numerical Weather Prediction Conference, Norfolk, VA, Aug. 19-23, 1996.

No. 124. Breaker, L. C., D. B. Gilhousen, H. L. Tolman and L. D. Burroughs, 1996: Initial Results from Long-Term Measurements of Atmospheric Humidity and Related Parameters in the Marine Boundary Layer at Two Locations in the Gulf of Mexico. NCEP Office Note No. 414.

No. 125. Yu, T. W., M. D. Iredell, and Y. Zhu, 1996: The Impact of ERS-1 Winds on NCEP Operational Numerical Weather Analyses and Forecast. Pre-print Numerical Weather Predicition Conference, Norfolk, VA, August 19-23, 1996.

No. 126. Burroughs, L. D., 1996: Marine Meteorological and Oceanographic Guidance Products from the National Centers for Environmental Prediction. Mariners Weather Log. (To be submitted).

No. 127. Lobocki, L., 1996: Coastal Ocean Forecasting System (COFS) System Description and User Guides. Technical Note.

No. 128. WAS NOT PUBLISHED

No. 129. Chailkov, D., 1996: A Global Ocean Model. Technical Note.

No. 130. Yu, T.W., 1996: Applications of SSM/I Wind Speed Data to NCEP Regional Analyses. Technical Note.

No. 131. Chailkov, D. and D. Sheinin, 1996: Direct Modeling of 1-D Nonlinear Potential Waves. Advances in Fluid Mechanics Series: Nonlinear Ocean Waves (submitted).

No. 132. Krasnopolsky, V. M., W. H. Gemmill, L. C. Breaker, and V. Y. Raizer, 1996: SSM/I Wind Speed Retrieval Algorithm with Improved Performance at Higher Wind Speed. Remote Sensing of Environment (submitted).

No. 133. Yu, T. W., 1996: The Effect of Drifting Buoy Data on NCEP Numerical Weather Forecast. Technical Note.

No. 134. Krasnopolsky, V. M., 1996: A Neural Network Forward Model for Direct Assimilation of SSM/I Brightness Temperatures into Atmospheric Models. CAS/JSC Working Group on Numerical Experimentation (in press).

No. 135. Krasnopolsky, V. M., W. H. Gemmill, and L. C. Breaker, 1996: A New Neural Network Transfer for SSM/I Retrievals. CAS/JSC Working Group on Numerical Experimentation (in press).

No. 136. Krasnopolsky, V. M., 1996: NN Solutions for Forward & Inverse Problems in Satellite Remote Sensing. 1997 International Conference on Neural Networks (ICNN 97). (submitted).

No. 137. Krasnopolsky, V. M., 1996: A New Neural Network Transfer Function for SSM/I Based on an Expanded Neural Network Architecture. Technical Note.

No. 138. Chailkov, D. C., L. C. Breaker, and L. Lobocki, 1996: Parameterization of Mixing in Upper Ocean. Technical Note.

No. 139. Chailkov, D. C., and D. Sheinin, 1996: Numerical Modeling of Surface Waves Based on Principal Equations of Potential Wave Dynamics. Technical Note.


DEPARTMENT OF COMMERCE
UNITED STATES OF AMERICA